HHS Public Access

Author manuscript

J Immunol. Author manuscript; available in PMC 2021 September 15.

Published in final edited form as:

J Immunol. 2020 September 15; 205(6): 1695–1708. doi:10.4049/jimmunol.2000530.

Innate lymphoid system is a critical player in the manifestation of muco-inflammatory airway disease in mice.

Brandon W Lewis[*], **Ishita Choudhary**[*], **Kshitiz Paudel**[*], **Yun Mao**[*], **Rahul Sharma**[†], **Yong Wang**[‡], **Jessy S Deshane**[‡], **Richard C Boucher**[§], **Sonika Patial**[*], **Yogesh Saini**[*,¶]

[*]Department of Comparative Biomedical Sciences, School of Veterinary Medicine, Louisiana State University, Baton Rouge, LA 70803, USA.

[‡]Department of Medicine, University of Alabama at Birmingham, Birmingham, AL 35294, USA.

[§]Marsico Lung Institute/University of North Carolina Cystic Fibrosis Center, School of Medicine, University of North Carolina at Chapel Hill, Chapel Hill, NC 27599, USA.

[†]National Hansen's Disease Program, School of Veterinary Medicine, Louisiana State University, Baton Rouge, LA 70803, USA.

Abstract

Innate lymphoid and adaptive immune cells are known to regulate epithelial responses, including mucous cell metaplasia (MCM), but their roles in muco-inflammatory airway diseases, such as cystic fibrosis (CF), remain unknown. *Scnn1b*-Tg+ (Tg+) mice, that recapitulate CF-like muco-inflammatory airway disease, deficient in innate lymphoid ($Il2rg^{KO}$), adaptive immune ($Rag1^{KO}$), or both systems ($Il2rg^{KO}/Rag1^{KO}$), were employed to investigate their respective contributions in the pathogenesis of muco-inflammatory airway disease. As previously reported, immunocompetent Tg+ juveniles exhibited spontaneous neonatal bacterial infections with robust muco-inflammatory features, including elevated expression of *Th2*-associated markers accompanied by MCM, elevated MUC5B expression, and airway mucus obstruction. The bacterial burden was increased in $Il2rg^{KO/}$Tg+ juveniles but returned to significantly lower levels in $Il2rg^{KO}/Rag1^{KO}$/Tg+ juveniles. Mechanistically, this improvement reflected reduced production of adaptive immunity-derived IL-10 and, in turn, increased activation of macrophages. While all the muco-inflammatory features were comparable between the immunocompetent Tg+ and $Rag1^{KO}$/Tg+ juveniles, the $Il2rg^{KO}$/Tg+ and $Il2rg^{KO}/Rag1^{KO}$/Tg+ juveniles exhibited suppressed expression levels of *Th2* markers, diminished MCM, suppressed MUC5B expression, and reduced mucus obstruction. Collectively, these data indicate that, in the context of airway mucus obstruction, the adaptive immune system suppresses antibacterial macrophage activation, whereas the innate lymphoid system contributes to MCM, mucin production, and mucus obstruction.

[¶]**Corresponding author:** *Yogesh Saini, BVSc & AH, MVSc, PhD,* Department of Comparative Biomedical Sciences, School of Veterinary Medicine, Louisiana State University, Baton Rouge, LA 70803, USA, Phone: 225-578-9143, Fax: 225-578-9895, ysaini@lsu.edu.

Author Contributions

Y. Saini and S. Patial conceived and designed the research; B.W. Lewis, and Y. Saini maintained the animal colony, conducted animal necropsies, and performed BALF cellularity assays; B.W. Lewis, R. Sharma, I Choudhary, K. Paudel, Y. Mao, Y. Wang, S. Patial, and Y. Saini performed cytokine, ELISA, gene expression assays, flow cytometry, microbiological, and histopathological experiments; S. Patial performed histopathological analyses; B.W. Lewis, J. S. Deshane, R.C. Boucher, S. Patial, and Y. Saini wrote and reviewed the manuscript for intellectual contents.

Keywords

Mucus Obstruction; Mucous cell metaplasia; Bacterial clearance; IL-10; Mucins

Introduction

In the healthy respiratory tract, the inhaled biotic or abiotic materials and host-derived end-products are effectively cleared by a coordinated effort of the airway mucociliary clearance (MCC) system, resident immune cells, and secreted antimicrobial peptides (1). Cystic fibrosis (CF), a muco-inflammatory lung disease, is characterized by airway surface liquid (ASL) layer depletion, excessive mucus production, mucus obstruction, impaired mucociliary clearance, and airway inflammation (2). As a consequence of impaired mucociliary clearance, CF patients are vulnerable to bacterial infections and pulmonary exacerbations due to viral infections (3). Our understanding of the molecular and cellular pathways leading to excessive mucus production in muco-inflammatory disease is incomplete, and a possibility of therapeutic inhibition of these pathways to ameliorate impaired mucociliary clearance remains untested in experimental animal models.

The *Scnn1b*-Tg+ (Tg+) mouse model of muco-inflammatory lung disease overexpresses the sodium channel non-voltage gated 1, β subunit (*Scnn1b*) transgene in club-cell specific protein (CCSP) expressing epithelial cells. *Scnn1b* transgene overexpression produces ASL layer depletion, impaired mucociliary clearance, excessive mucus accumulation, and airway inflammation (4–7). As a result of mucus obstruction, Tg+ neonates contract airspace bacterial infection in early postnatal life (6). The Tg+ neonatal mice exhibit robust *Th2* responses with marked mucous cell metaplasia (MCM) and mucus obstruction (7, 8). Our recent data indicate the deficiency of interleukin 33 (IL-33), a regulator of *Th2* immunity, in Tg+ juveniles resulted in a remarkable attenuation of MCM, but with no obvious amelioration of mucus obstruction (9). Since mucus production has also been associated with T-helper type I (*Th1)* inflammatory responses in the lungs (10), it remains unclear whether non-*Th2* adaptive and innate lymphoid cells (ILCs) are involved in mucus production and/or obstruction in Tg+ mice.

In this study, we have tested the hypotheses that innate lymphoid and adaptive immune cells are essential for the manifestation of MCM and mucus secretory responses in Tg+ mice. ILCs, i.e., ILC1, ILC2, ILC3, and NK cells, represent the amnestic equivalence of adaptive immune cells *Th1, Th2, Th17, cytotoxic T* cells, respectively (11–14). The availability of *Interleukin-2 receptor-gamma (Il2rg)* and *Recombination activating gene 1 (Rag1)* knockout strains allow complete ablation of innate lymphoid (15) and adaptive immune systems, respectively (16). To investigate the contribution of, and interactions between, the innate lymphoid and adaptive immune systems in muco-inflammatory lung disease in Tg+ mice, innate lymphoid cell -deficient ($Il2rg^{KO}$), adaptive immune cell -deficient ($Rag1^{KO}$), and innate lymphoid/adaptive immune cell -deficient ($Il2rg^{KO}/Rag1^{KO}$) mice were generated on WT (absence of *Scnn1b transgene*) and Tg+ (presence of *Scnn1b transgene*) backgrounds. Designated muco-inflammatory endpoints including airspace bacterial burden, airway inflammation, mucus obstruction, MCM, and gene expression were examined. The results

from this study provide novel insights into the independent and combined contribution of the innate lymphoid and adaptive immune systems in the pathogenesis of muco-inflammatory lung disease in Tg+ mice.

Materials and Methods

Generation of transgenic mice and animal husbandry:

Scnn1b-Tg+ (Tg+) mice (*Tg(Scgb1a1-Scnn1b)6608Bouc/J*), *Il2rg*^{KO} (B6.129S4-Il2rg^{tm1Wjl}/J), and *Rag1*^{KO} (B6.129S7-Rag1^{tm1Mom}/J) were obtained from the Jackson Laboratory (Bar Harbor, ME). These three strains were crossbred to generate innate lymphoid cell-deficient (*Il2rg*^{KO}), adaptive immune cell-deficient (*Rag1*^{KO}), and combined innate lymphoid and adaptive immune cell-deficient (*Il2rg*^{KO}/*Rag1*^{KO}) wildtype (WT) and Tg+ mice. To generate littermates of various genotypic combinations, double heterozygous (*Il2rg*^{HET}/*Rag1*^{HET}) *Scnn1b*-Tg+ females were mated with double knockout (*Il2rg*^{KO}/*Rag1*^{KO}) WT males. In reciprocal crossing, double heterozygous (*Il2rg*^{HET}/*Rag1*^{HET}) Tg+ males were mated with double knockout (*Il2rg*^{KO}/*Rag1*^{KO}) WT females. Of note, the *Il2rg* gene is located only on X-chromosomes, although the *Il2rg*-sufficient males are hemizygous at *Il2rg* locus, for sake of simplicity, we will address both *Il2rg*-sufficient males and *Il2rg*-heterozygous females as *Il2rg*^{HET}. Genotyping for all mice was performed by polymerase chain reaction (PCR) for the determination of *Scnn1b*-Tg+, *Il2rg*, and *Rag1 alleles* (data not shown). Mice were maintained in individually ventilated, hot-washed cages on a 12-hour dark/light cycle and were supplied regular diet and water *ad libitum*. Mice were housed in a specific pathogen-free facility at the Division of Laboratory Animal Medicine (DLAM) at Louisiana State University, Baton Rouge. All animal use procedures were approved by the Institutional Animal Care and Use Committee (IACUC) of Louisiana State University.

Flow Cytometry:

Heart and lungs were removed *en bloc* from 10-day old WT and Tg+ littermates. Lungs were perfused by flushing 5ml of phosphate buffered saline (PBS) through the right ventricle of the heart. Perfused lungs were transferred to C-tubes (Miltenyi Biotec, Gladbach, Germany) and digested in DMEM/F12 medium containing collagenase Type IV (Worthington, Lakewood, NJ) and DNAase (Sigma Aldrich, St. Louis, MO). Lung tissues were homogenized using a GentleMACS dissociator (Miltenyi Biotec, Gladbach, Germany) followed by incubation on a rocker at 37°C. Cell suspensions were filtered through a 70μm nylon cell strainer followed by centrifugation at 300 X g for 10 minutes. Cells were resuspended in 10ml of DMEM/F12 medium and counted using TC20 automated cell counter (Bio-Rad, Hercules, CA) with a gating size of 6–22nm.

For Th stimulation, ~2 million cells were incubated in DMEM/F12 medium containing a leukocyte activation cocktail (BD Biosciences, San Jose, CA), a protein transport inhibitor containing monensin (BD Biosciences, San Jose, CA), and 10% fetal bovine serum (FBS) at 37°C for three hours. Cells were collected and permeabilized/fixed using Fixation/Permeabilization buffer and 1X Permeabilization/Wash Buffer (BD Biosciences, San Jose, CA). Cells were suspended in 200μl of PBS with 3% FBS.

Unstimulated cells were centrifuged at 300xg for 5 minutes and the cell pellets were resuspended in 2ml of PBS. Cells were fixed in 4% paraformaldehyde solution (Electron Microscope Sciences, Hatfield, PA) followed by a wash and final resuspension in 200μl of PBS with 3% FBS. Single cell suspensions were stained with various fluorochrome - conjugated anti-mouse monoclonal antibodies for cellular phenotyping as follows: Lin (CD3, B220, CD11b, TER-119, Gr-1, CD11c, NK1.1, FceR1α, CD8a, CD4), CD45, CD90, IL-33R, CD278, CD3, CD4, CD25, Foxp3, NK1.1, CD127, RORrt, Eomes, IFN-γ, IL-4, and IL-17. Data were acquired using a BD LSRII flow cytometer (BD Biosciences, San Jose, CA) and analyzed using FlowJo software (v9.2).

Bronchoalveolar lavage (BAL) and tissue harvesting:

Neonates [postnatal day (PND) 6–7] and juveniles (PND22) were anesthetized and aseptic bronchoalveolar lavage (BAL) fluid was harvested as described previously (17). Unlavaged left lung lobes were stored in 10% neutral buffered formalin (NBF) for histopathological analyses. Cell-free BAL fluid (BALF) was stored at −80°C for cytokine analyses. Right lung lobes were snap-frozen and stored at −80°C for gene expression analyses.

BAL cellularity: Total and differential cell counts were measured in BALF, as described previously (8).

Cytokine analyses: Cell-free BALF was assayed for mouse IL-4, IL-5, IL-10, IL-13, keratinocyte chemoattractant (KC; CXCL1), MIP-2 (CXCL2), G-CSF, MCP-1 (CCL2), IP-10 (CXCL10), and TNFα concentrations using a Luminex XMAP-based assay (MCYTOMAG-70K), as per the manufacturer's instructions (EMD Millipore, Billerica, MA).

BAL microbiology: For the determination of bacterial burden in airspaces, aseptically harvested BAL was serially diluted onto Columbia Blood Agar (CBA) plates (Hardy Diagnostics, Santa Maria, CA) and incubated anaerobically in a candle jar for 48 hours at 37°C as previously described (6, 17). Colony forming units (CFUs) were enumerated and morphologically distinct colonies were amplified via re-streaking onto CBA plates. Bacterial samples were heat -inactivated for 3 minutes at 100°C and genomic DNA was extracted as previously described (8).

16S gene sequencing: Bacterial genomic DNA was extracted as previously described (8). Genomic DNA was processed and analyzed by sequencing hyper-variable regions of the 16S ribosomal RNA gene by using the following primer pairs: 27F: 5'-AGAGTTTGATCMTGGCTCAG-3' and 1492R: 5'-TACGGYTACCTTGTTACGACTT-3'; 518F: 5'-CAGCAGCCGCGGTAATACG-3' and 800R: 5'-TACCAGGGTATCTAATCC-3' using LongAMP Taq 2X Master Mix (New England Biolabs, Ipswitch, MA). Sequencing was performed on Applied Biosystems 3720XL DNA sequencer (Psomagen, Rockville, MA). Genus or species of bacterial isolates were identified based on sequence homology using the 16S rRNA sequence database at NCBI using the Basic Local Alignment Search Tool (BLAST).

Histopathological Analyses:

Unlavaged left lung lobes were formalin-fixed, paraffin-embedded, sectioned, and processed for histopathological analyses. Histological slides stained with hematoxylin and eosin (H&E) were used to assess cellular and morphological alterations. Alcian blue-periodic acid Schiff (AB-PAS) stained sections were used to determine intracellular as well as extracellular accumulation of mucopolysaccharide substances. Using Nikon camera software, mucous cell metaplasia analyses were performed by quantifying the number of mucous cells per millimeter (mm) of basement membrane, under 40X objective of ECLIPSE Ci-L microscope with DS-Fi2 camera attachment (Nikon, Melville, NY). To compare other histopathological parameters, a previously described histological semi-quantitative grading strategy was employed by a blinded board-certified anatomic pathologist (18).

The degree of mucus obstruction was accessed by quantifying percent obstruction of large airways. Briefly, photomicrographs of lung section containing airway lumens with maximum obstruction were captured under 20X objective of ECLIPSE Ci-L microscope with DS-Fi2 camera attachment (Nikon, Melville, NY). Using image J software, the captured images were processed to determine the percentage of total luminal area obliterated by the AB-PAS stained mucopolysaccharide content (19).

Immunohistochemistry for MUC5B and MUC5AC:

Formalin-fixed paraffin-embedded lung sections were used for immunohistochemical localization of MUC5AC and MUC5B. 5μm sections were deparaffinized with CitriSolv (2 × 5 min each) and were rehydrated with graded ethanol (100, 95, 70, 30%, distilled water; 3 min each). Antigen retrieval was performed using a citrate buffer-based heat-induced antigen-retrieval method (heating slides in 10mM sodium citrate solution [with 0.05% Tween 20; pH 6.0] at 95–100°C for 30 min, followed by cooling to room temperature). Quenching for endogenous peroxidases was performed with 3% hydrogen peroxide in deionized water for 10 min at room temperature, followed by a PBS wash. After blocking with 3% goat serum for 30 min, sections were incubated for 2 h at room temperature with rabbit polyclonal MUC5B primary antibodies (UNC223; University of North Carolina, Chapel Hill, NC), MUC5AC primary antibodies (UNC294; University of North Carolina, Chapel Hill, NC) and isotype control antibodies (Rabbit IgG; Jackson ImmunoResearch, West Grove, PA). The sections were then rinsed in PBS (2 × 5 min each) and processed using VECTASTAIN Elite ABC HRP Kit (Vector Laboratories, Burlingame, CA), followed by chromogenic substrate conversion to insoluble colored precipitate using ImmPACT NovaRED HRP substrate Kit (Vector Laboratories, Burlingame, CA). After a rinse in tap water, sections were counterstained with Gill's Hematoxylin-I, rinsed in de-ionized water, dehydrated with graded alcohol solutions, and coverslipped with VectaMount mounting media (H-5000, Vector Laboratories, Burlingame, CA)). Mounted slides were imaged by light microscopy (Nikon Ci-L microscope).

Macrophage surface area determination:

Differentially stained cytospins were used for macrophage surface area (μm^2) determination. On 20X objective of ECLIPSE Ci-L microscope with DS-Fi2 camera attachment (Nikon,

Melville, NY), the surface area of at least 200 macrophages/mouse was determined using Nikon camera software (Nikon, Melville, NY).

Intranasal aspiration:

To induce aspiration-induced bacterial infection, 10μl of sterile PBS was administered intranasally (5μl/nostril) in 2 days old pups for four consecutive days (PND2-5). In experimental groups, 200pg of recombinant IL-10 (Peprotech, Rocky Hill, NJ) dissolved in 10μl of PBS was administered.

Immunocytochemistry:

BALF cytospins were prepared and fixed with 10% NBF at room temperature for 20 minutes. Fixed cytospins were washed with PBS and permeabilized with 0.1%-Triton X100. After PBS washes, cytospins were incubated with Odyssey blocker (LI-COR Biosciences, Lincoln, NE) for 30 minutes at room temperature, following which the cytospins were incubated (overnight incubation at 4°C) with rabbit polyclonal antibodies against inducible nitric oxide synthase (iNOS) (1:250, ab15323, ABCAM Cambridge, MA). After PBS washes, cytospins were incubated (one hour at room temperature) with Alexa Fluor 594 labeled goat-anti -rabbit (Life technologies, Carlsbad, CA) secondary antibody. After nuclear staining (NucBlue, Life technologies, Carlsbad, CA), images were acquired on live cell imager (Zoe Fluorescent Cell Imager, Bio-Rad, Hercules, CA).

Gene Expression Analyses

Gene expression analyses were performed as previously described (8).

Statistical analyses

Significant differences among groups were determined using ANOVA followed by Tukey post hoc test for multiple comparisons. Non-parametric data were compared by the Kruskal-Wallis test with Dunn's post-test for multiple comparisons. Significant differences between the two groups were determined using Student's *t* test assuming unequal variance. A *p*-value of 0.05 was considered statistically significant. All data were expressed as mean ± SEM. GraphPad Prism 8.0 was used to perform statistical analyses (GraphPad Software, La Jolla, CA).

Results:

Immune cells associated with Th2 responses are elevated in Tg+ lungs

To quantify the relative levels of innate lymphoid cell (ILCs) subtypes (ILC1, ILC2, and ILC3) and their non-amnestic counterpart T helper-cell subtypes (*Th1, Th2, and Th17*), whole lung digests from 10 days old WT and *Scnn1b*-Tg+ (Tg+) mice were analyzed using flow cytometry. Although non-significant, the total counts for ILC2s ($CD45^+Lin^-CD90^+IL\text{-}33R^+CD278^+$) trended higher in Tg+ pups as compared to WT counterparts (Fig. 1A). Notably, these cells were present in a significantly higher proportion of total harvested cells in Tg+ pups as compared to WT counterparts (Fig. 1A). Consistent with ILC2s, the total counts were trending higher and the proportion of *Th2* cells ($CD3^+CD4^+IL\text{-}4^+$) was

also higher in Tg+ lungs as compared to WT lungs (Fig. 1B). The total counts and proportion of *Th1/Th2* hybrid cells were also elevated in Tg+ pups as compared to WT counterparts, but the differences were statistically insignificant (Supplemental Fig. 1B).

The total counts ($p=0.07$) and proportion of ILC1 ($p<0.05$) were lower in the Tg+ pups as compared to WT counterparts (Supplemental Fig. 2A). ILC3s were present at comparable proportions in both groups (Supplemental Fig. 2B). While total counts as well as the proportion of *Th1* cells were lower in Tg+ pups as compared to WT counterparts, the differences were not statistically significant (Supplemental Fig. 2C). Consistent with ILC3s, their non-amnestic equivalent, i.e., *Th17,* were also present at comparable proportions in both groups (Supplemental Fig. 2C). These data suggest that the *Th2* response-associated key cell type, i.e., ILC2 and *Th2*, are enriched in the lungs of 10-days old Tg+ mice.

Ablation of innate lymphoid immune cells results in increased bacterial burden, which is partially rescued by concomitant ablation of adaptive immune cells

Neonatal pups are prone to the aspiration of oropharyngeal secretions, along with microbes of oropharyngeal origin (6, 17). To determine whether the ablation of innate lymphoid system, adaptive immune system, or both systems affected the burden of aspirated oropharyngeal bacteria in neonates, aseptically harvested bronchoalveolar lavage fluid (BALF) from designated genetic strains were analyzed for bacterial burdens (Fig. 2A). While only ~ 38% immunocompetent WT ($Il2rg^{HET}/Rag1^{HET}$/WT) neonates (Postnatal day (PND) 6–7) had minimal levels of bacterial infection (mean CFUs = ~49), ~ 70% of $Il2rg^{KO}$/WT ($Il2rg^{KO}/Rag1^{HET}$/WT) neonates exhibited significantly increased bacterial burden (mean CFUs = $\sim 2.7 \times 10^3$) (Fig. 2A). In contrast, only ~18% of $Rag1^{KO}$/WT ($Il2rg^{HET}/Rag1^{KO}$/WT) neonates had minimal bacterial burden (mean CFUs= ~4.5) (Fig. 2A). Interestingly, compared to $Il2rg^{KO}$/WT pups, the $Il2rg^{KO}/Rag1^{KO}$/WT neonates had remarkably lower (p -value = 0.07) bacterial burden (mean CFUs= ~34; prevalence= ~25%), suggesting that the ablation of the adaptive immune system compensates for compromised bacterial clearance that was evident in $Il2rg^{KO}$/WT neonates (Fig. 2A).

As reported previously (6, 17), as compared to WT littermates, the immunocompetent Tg+ neonates had significantly higher spontaneous bacterial infections (CFUs=~ 1.9×10^3; prevalence = 100%). Next, we determined bacterial counts in the BALF from $Il2rg^{KO}$/Tg+, $Rag1^{KO}$/Tg+, and $Il2rg^{KO}/Rag1^{KO}$/Tg+ neonates (Fig. 2A). Although not significantly different, all the $Il2rg^{KO}$/Tg+ neonates had a higher bacterial burden (CFUs=~ 5.6×10^3; prevalence = ~100%), as compared to immunocompetent Tg+ neonates (Fig. 2A). The $Rag1^{KO}$/Tg+ neonates had lower bacterial burden (CFUs=~ 1.0×10^3; prevalence = ~87%; p value= 0.06) compared to $Il2rg^{KO}$/Tg+ neonates (Fig. 2A). As compared to $Il2rg^{KO}$/Tg+ neonates, the ablation of the adaptive immune system in innate lymphoid-deficient *Scnn1b*-Tg+ neonates ($Il2rg^{KO}/Rag1^{KO}$/Tg+) resulted in lower prevalence (~69%) with lower bacterial burden (CFUs=~ 1.6×10^3) (Fig. 2A).

To determine if the loss of the innate lymphoid immunity results in more persistent infections, BALF was aseptically harvested from juveniles (PND 22) and microaerophilic CFUs were enumerated. The early neonatal infection was mostly resolved in WT juveniles at PND 22, with the exception of one mouse with minimal infection (Fig. 2B). As compared

to their higher bacterial burden at PND 6–7, ~42% of the *Il2rg*^{KO}/WT juveniles had bacterial burden at lower level (mean CFUs= ~8.2). Approximately, ~44% of *Rag1*^{KO}/WT and ~33% of *Il2rg*^{KO}/*Rag1*^{KO}/WT juveniles also bacterial burden of ~16 and ~10 CFU, respectively. The spontaneous bacterial infection that was highly prevalent in *Scnn1b*-Tg+ neonates was significantly cleared in ~57% of *Scnn1b*-Tg+ juveniles (CFUs= ~ 87) (Fig. 2B). While ~ 83% *Il2rg*^{KO}/Tg+ juveniles still had a significantly higher bacterial burden (CFUs=~ 1.8 × 10^3), ~ 45% *Rag1*^{KO}/Tg+ juveniles exhibited a relatively lower bacterial burden (CFUs=~ 258) (Fig. 2B). Further, ~67% *Il2rg*^{KO}/*Rag1*^{KO}/Tg+ juveniles had also relatively lower bacterial burden (CFUs=~ 588), as compared to *Il2rg*^{KO}/Tg+ juveniles.

To determine the effect of ablation of the immune systems on the diversity of microaerophilic microflora, bacterial 16S sequencing was performed on aseptically harvested CFUs. The infected pups from the eight experimental groups had *Pasteurella* sp. as a common bacterium (Fig. 2C). Except three infected mice in immunocompetent WT group, none of the infected mice in *Il2rg*^{KO}/WT, *Rag1*^{KO}/WT, *and Il2rg*^{KO}/*Rag1*^{KO}/WT had *Streptococcus* sp. infection. However, *Streptococcus* sp. infection was prevalent in all the four groups on Tg+ background. Except for two incidences of bacterial infection due to *Achromabacter* sp. and *Bacillus* sp., infected pups in all the four Tg+ groups exhibited a comparable diversity of microflora (Fig. 2C). These data suggest that the individual or combined loss of innate lymphoid and adaptive immune system does not affect the diversity of microaerophilic microflora in Tg+ mice.

Concomitant ablation of innate lymphoid and adaptive immune cells abolishes IL-10-mediated immunosuppression of proinflammatory macrophage activation in Tg+ neonates

IL-10 is a known immunosuppressive anti-inflammatory cytokine that is involved in reduced bacterial clearance through suppression of antibacterial functions of various cells, including T helper subsets, macrophages, dendritic cells, and neutrophils (20–23). Cells of both immune systems, i.e., innate lymphoid and adaptive immune system, as well as macrophages and dendritic cells are known producers of IL-10 (24, 25). To investigate the mechanism that accounts for the better clearance of bacterial infection in *Il2rg*^{KO}/*Rag1*^{KO} mice, we hypothesized that reduction in the immunosuppressive effect of IL-10 on proinflammatory macrophage activation contributed to improved bacterial clearance. Accordingly, we assayed IL-10 levels in the BALF of all the experimental groups at PND 6–7 (Fig. 3A). Although nonsignificant, the BALF from *Il2rg*^{KO}/WT had higher levels of IL-10 (mean 14.24 ± 7.63 pg/ml) as compared to immunocompetent WT neonates (mean 1.17 ± 0.23 pg/ml) (Fig. 3A). As compared to the *Il2rg*^{KO}/WT neonates, the *Rag1*^{KO}/WT (mean 1.13 ± 0.36 pg/ml) and *Il2rg*^{KO}/*Rag1*^{KO}/WT (mean 2.39 ± 1.27 pg/ml) neonates had relatively lower BALF levels of IL-10 (Fig. 3A). A similar trend was seen among the four groups on Tg+ background. The immunocompetent Tg+ (mean 95.05 ± 61.16 pg/ml) and *Il2rg*^{KO}/Tg+ (mean 418.9 ± 405.5 pg/ml) neonates had comparable levels of IL-10 that were significantly elevated as compared to immunocompetent WT neonates (Fig. 3A). As compared to the *Il2rg*^{KO}/Tg+ neonates, the *Rag1*^{KO}/Tg+ had relatively lower IL-10 levels (mean 14.18 ± 8.23 pg/ml) without statistical significance, and the IL-10 levels were significantly reduced in *Il2rg*^{KO}/*Rag1*^{KO}/Tg+ neonates (mean 2.47 ± 1.34 pg/ml) (Fig. 3A).

To test whether the beneficial effect of innate lymphoid and adaptive immune deficiency on bacterial clearance is caused due to reduced IL-10 contents and enhanced phagocytotic clearance of bacteria, we introduced bacterial infection in the *Il2rg*^{KO}/*Rag1*^{KO}/WT neonates through intranasal administration model, as delineated in Fig. 3B. In this approach, 10μl sterile PBS or IL-10 (200pg in 10μl of PBS) was administered intranasally (5μl/nostril) from PND 2–5. As compared to PBS-treated pups, the IL-10 treated pups had ~2 folds higher bacterial counts (Fig. 3C; **p=0.051**). The total (Fig. 3D; **p<0.01**), neutrophil (Fig. 3E; **p<0.01**), and macrophage (Fig. 3F; **p=0.12**) counts were also elevated in IL-10 treated versus PBS-treated neonates.

To determine the effect of IL-10 on macrophage activation, macrophage sizes were estimated. While PBS-treated *Il2rg*^{KO}/*Rag1*^{KO}/WT neonates had macrophages with significantly larger sizes, macrophages from IL-10-treated *Il2rg*^{KO}/*Rag1*^{KO}/WT neonates were relatively smaller (Fig. 3G). Approximately 43% of BALF macrophages in PBS-treated *Il2rg*^{KO}/*Rag1*^{KO}/WT neonates were above 400μm^2 (Fig. 3H); in contrast, only ~ 13% of BALF macrophages in IL-10-treated *Il2rg*^{KO}/*Rag1*^{KO}/WT neonates were above 400μm^2 (Fig. 3I). Further, we assessed the proportion of inducible nitric oxide synthase (iNOS) (a marker of classically activated bactericidal macrophages) positive macrophages in PBS-treated or IL-10-treated *Il2rg*^{KO}/*Rag1*^{KO}/WT neonates. As expected, BALF from IL-10-treated *Il2rg*^{KO}/*Rag1*^{KO}/WT neonates had a significantly lesser proportion of iNOS positive cells (Fig. 3J). These data suggest that morphologically (increased size) and functionally (iNOS-positive) activated macrophages are suppressed by IL-10.

Ablation of innate lymphoid and adaptive immune cells differentially affect immune cell recruitment and inflammatory mediators in WT and Scnn1b-Tg+ juveniles

We next determined if the ablation of innate lymphoid system, adaptive immune system, or a combination of both systems affected the immune cell composition, numbers, or type of immune cells in the BALF from immunocompetent WT, *Il2rg*^{KO}/WT, *Rag1*^{KO}/WT, and *Il2rg*^{KO}/*Rag1*^{KO}/WT juveniles. In the absence of *Scnn1b* transgene, there was no significant difference in the total number of cells between the juveniles (Fig. 4A). In addition, the ablation of innate lymphoid system, adaptive immune system, or a combination of both systems did not result in significant alterations in the total number of macrophages (Fig. 4B), neutrophils (Fig. 4C), eosinophils (Fig. 4D), and lymphocytes (Fig. 4E).

The total numbers as well as types of immune cells were also determined in the BALF of immunocompetent Tg+, *Il2rg*^{KO}/Tg+, *Rag1*^{KO}/Tg+, and *Il2rg*^{KO}/*Rag1*^{KO}/Tg+ juveniles. Compared to their WT counterparts, except immunocompetent Tg+, all the Tg+ groups had significantly increased numbers of total cells (Fig. 4A). Among the four Tg+ groups, there were no significant differences in the total cell (Fig. 4A), macrophage (Fig. 4B), neutrophil (Fig. 4C), or lymphocyte (Fig. 4E) counts. As compared to the immunocompetent Tg+ juveniles; while the *Rag1*^{KO}/Tg+ juveniles had equivalent eosinophil counts, the *Il2rg*^{KO}/Tg + and *Il2rg*^{KO}/*Rag1*^{KO}/Tg+ juveniles had significantly reduced eosinophil counts (Fig. 4D).

Despite comparable numbers of macrophages in the four groups on WT as well as Tg+ backgrounds, we observed genotype-dependent significant changes in surface area of macrophages. The proportions of macrophages with surface area greater than 400μm^2 were

~4%, 0%, 10%, 12% in immunocompetent WT, *Il2rg*^{KO}/WT, *Rag1*^{KO}/WT, and *Il2rg*^{KO}/*Rag1*^{KO}/WT juveniles, respectively (Fig. 4F; Supplemental Fig. 3A–D). As previously reported (6), a significant proportion of macrophages were morphologically activated, as indicated by their sizes, in all the four groups with Tg+ status. The genotype-dependent trends in morphological macrophage activation observed on WT background was also evident in groups on Tg+ background, i.e., ~41%, ~13%, ~65%, ~68% macrophages in Tg+, *Il2rg*^{KO}/Tg+, *Rag1*^{KO}/Tg+, and *Il2rg*^{KO}/*Rag1*^{KO}/Tg+ juveniles, respectively, had surface area greater than 400μm^2 (Fig. 4F; Supplemental Fig. 3E–H). These data suggest greater morphological activation in the absence of adaptive immune system but also reduced activation in the absence of innate lymphoid system.

To identify the roles of innate lymphoid versus adaptive immune system in the establishment of cytokine/chemokine concentrations in the airspaces of WT and *Scnn1b*-Tg+ mice, we assessed the concentrations of designated chemokines and inflammatory mediators in the BALF from immunocompetent, *Il2rg*^{KO}, *Rag1*^{KO}, and *Il2rg*^{KO}/*Rag1*^{KO} mice. Neutrophil chemoattractants, i.e., KC (CXCL1), MIP-2 (CXCL2), and G-CSF, were undetectable in the BALF from WT, *Il2rg*^{KO}/WT, *Rag1*^{KO}/WT, and *Il2rg*^{KO}/*Rag1*^{KO}/WT juveniles (Fig. 4G–I). As compared to their WT counterparts, BALF levels of three neutrophil chemoattractants were significantly increased in the BALF from immunocompetent Tg+ and *Rag1*^{KO}/Tg+ juveniles (Fig. 4G–I). However, as compared to immunocompetent Tg+, the levels of neutrophil chemoattractants were significantly elevated in the BALF from *Il2rg*^{KO}/Tg+ and *Il2rg*^{KO}/*Rag1*^{KO}/Tg+ juveniles. As compared to *Rag1*^{KO}/Tg+ juveniles, the *Il2rg*^{KO}/*Rag1*^{KO}/Tg+ juveniles had significantly elevated levels of all the three neutrophil chemoattractants (Fig. 4G–I).

IL-5, a key cytokine involved in the maturation, survival and recruitment of eosinophils, was undetectable in the in BALF from immunocompetent WT, *Il2rg*^{KO}/WT, *Rag1*^{KO}/WT, and *Il2rg*^{KO}/*Rag1*^{KO} /WT juveniles (Fig. 4J). As compared with their WT counterparts, BALF levels of IL-5 were elevated in immunocompetent Tg+ and *Rag1*^{KO}/Tg+ juveniles, a trend also shown by eosinophil counts in the BALF of these groups (Fig. 4D). In contrast, the BALF IL-5 levels were non-detectable in *Il2rg*^{KO}/Tg+ and *Il2rg*^{KO}/*Rag1*^{KO}/Tg+ juveniles (Fig. 4J).

Ablation of innate lymphoid, but not of adaptive immunity, suppresses molecular signatures of Th2 inflammation in the airspaces of Tg+ juveniles

To determine the contributions of innate lymphoid and adaptive immune systems in *Th2* inflammation in Tg+ mice, we assessed molecular signatures of *Th2* inflammation in immunocompetent, *Il2rg*^{KO}, *Rag1*^{KO}, and *Il2rg*^{KO}/*Rag1*^{KO} juveniles on WT and Tg+ backgrounds. While BALF levels of IL-13, a primary *Th2* cytokine, were below detection limits in all the eight experimental groups (data not shown), the expression levels of *Il13* mRNA were elevated in the immunocompetent Tg+ as well as *Rag1*^{KO}/Tg+ juveniles (Fig. 5A). The transcript levels for *Il13* were suppressed in *Il2rg*^{KO}/Tg+ and *Il2rg*^{KO}/*Rag1*^{KO}/Tg+ juveniles (Fig. 5A). The BALF levels of IL-4, another primary *Th2* cytokine, were significantly elevated in the immunocompetent Tg+ and *Rag1*^{KO}/Tg+ groups (Fig. 5B). The BALF IL-4 levels were below the detection limits in the rest of the six experimental groups.

The gene expression levels of *Il4* were at the baseline in the *Il2rg*^{KO}, *Rag1*^{KO}, and *Il2rg*^{KO}/*Rag1*^{KO} juveniles (Fig. 5C). The immunocompetent Tg+ juveniles had significantly elevated levels of *Il4*, which were significantly reduced in *Il2rg*^{KO}/Tg+ and *Il2rg*^{KO}/*Rag1*^{KO}/Tg+ juveniles (Fig. 5C).

Next, we assessed gene expression levels for *Th2* inflammation-associated signatures, i.e., *Slc26a4 (Pendrin), Clca1/3 (Gob5), Retnla (Fizz1), Chi3l4 (Ym2),* and *Mmp12* which have been previously reported in *Scnn1b*-Tg+ mice (7–9). In the absence of *Scnn1b* transgene, the gene expression levels for these signatures were at baseline in all the four groups [e.g., *Slc26a4* (Fig. 5D), *Clca1/3* (Fig. 5E), *Retnla* (Fig. 5F) *Chi3l4* (Fig. 5G), and *Mmp12* (Fig. 5H)]. Both, immunocompetent Tg+ and *Rag1*^{KO}/Tg+ groups had significantly elevated levels of these gene signatures. In contrast to immunocompetent Tg+, the expression levels of all the five genes were significantly reduced in the *Il2rg*^{KO}/Tg+ and *Il2rg*^{KO}/*Rag1*^{KO}/Tg+ juveniles (Fig. 5C–H).

Exaggerated inflammatory injury markers in the BALF of Il2rg^{KO}/Tg+ juveniles dampen in the absence of adaptive immune response

Proinflammatory mediators, i.e., IP-10 (CXCL10), TNFα, MCP-1 (CCL2), are present at significantly elevated levels in the BALF of immunocompetent Tg+ mice (8, 9, 17). Consistent with these reports, the immunocompetent Tg+ mice possessed these mediators at a concentration higher than those in immunocompetent, *Il2rg*^{KO}, *Rag1*^{KO}, and *Il2rg*^{KO}/*Rag1*^{KO} juveniles on WT background. As compared to immunocompetent Tg+ mice, the BALF levels for IP-10 and TNFα were significantly elevated in *Il2rg*^{KO}/Tg+ juveniles (Supplemental Fig. 3I–K). The BALF levels for IP-10 and TNFα were significantly reduced in the *Rag1*^{KO}/Tg+ juveniles versus *Il2rg*^{KO}/Tg+ juveniles. As compared to *Il2rg*^{KO}/Tg+ juveniles, while the *Il2rg*^{KO}/*Rag1*^{KO}/Tg+ juveniles had significantly reduced levels of IP-10, the contents for TNFα ($p=0.12$) and MCP-1 ($p=0.19$) were reduced but without statistical significance (Supplemental Fig. 3I–K).

Ablation of innate lymphoid, but not of adaptive immunity, suppresses mucous cell metaplasia in Tg+ juveniles

To determine the effect of ablation of the two immune systems on the mucous cell metaplasia responses, a consistent feature of *Scnn1b*-Tg+ airway pathology (4, 5), we assessed histological signs and molecular signatures of MCM in all the eight experimental groups. As previously reported (18), the immunocompetent WT juveniles had significant linear density (~ 33 cells/mm of basement membrane) of Alcian blue-periodic acid Schiff stained (AB-PAS^{+}) cells, consistent with intracellular mucopolysaccharide contents (Fig. 6A–B). While the *Il2rg*^{KO}/WT (~ 3 cells/mm of basement membrane) and *Il2rg*^{KO}/*Rag1*^{KO}/WT (~ 4 cells/mm of basement membrane) juveniles were completely devoid of AB-PAS^{+} cells, the *Rag1*^{KO}/WT juveniles had AB-PAS^{+} cells (~ 29 cells/mm of basement membrane) similar to immunocompetent WT juveniles (Fig. 6A–B).

As reported previously (4, 5), as compared to immunocompetent WT littermates, the immunocompetent Tg+ juveniles had significantly greater linear density (~ 62cells/mm of basement membrane) of AB-PAS^{+} cells. As observed on the WT background, while the

Rag1^{KO}/Tg+ juveniles had equivalent numbers of AB-PAS^{+} cells (~ 50 cells/mm of basement membrane) as immunocompetent Tg+ juveniles (Fig. 6A–B); the loss of innate lymphoid immunity significantly reduced the linear density of AB-PAS^{+} cells in *Il2rg*^{KO}/Tg + (~ 6 cells/mm of basement membrane) and *Il2rg*^{KO}/*Rag1*^{KO}/Tg+ (~ 10 cells/mm of basement membrane) juveniles (Fig. 6A–B).

Transcript signatures associated with the molecular programming of MCM including *Spdef, Agr2, Tff2, and Gata3* were assessed in total RNA harvested from the lungs of all the eight experimental groups (Fig. 6C–F). In the four experimental groups on WT background, only *Tff2, Agr2,* and *Gata3*, were upregulated in two groups with a greater linear density of AB-PAS^{+} cells, i.e., immunocompetent WT and *Rag1*^{KO}/WT juveniles (Fig. 6C–F). The immunocompetent Tg+ and *Rag1*^{KO}/Tg+ juveniles had comparable levels of expression for *Spdef, Agr2, Tff2, and Gata3.* As compared to immunocompetent Tg+ and *Rag1*^{KO}/Tg+ juveniles, the *Il2rg*^{KO}/Tg+ juveniles showed relatively lower expression levels of *Spdef, Agr2, Tff2,* and *Gata3.* These reductions were significant in *Il2rg*^{KO}/*Rag1*^{KO}/Tg+ juveniles (Fig. 6C–F)

Ablation of innate lymphoid system mitigates mucus obstruction in Tg+ juveniles

To determine the effect of ablation of the two immune systems on the mucus obstruction, a consistent feature of *Scnn1b*-Tg+ airway pathology (4, 5), we examined lung sections from all the eight experimental groups. As expected, four experimental groups on WT background had no signs of mucopolysaccharide contents in the airway lumens (Fig. 7B). In agreement with previous reports (4, 5), the immunocompetent Tg+ juveniles had consistent signs of mucus obstruction in the airways (Fig. 7A–B). The *Rag1*^{KO}/Tg+ juveniles also had obstruction comparable to the immunocompetent Tg+ juveniles. Both *Il2rg*^{KO}/Tg+ and *Il2rg*^{KO}/*Rag1*^{KO}/Tg+ juveniles, consistent with their absence of MCM responses, had reduced mucus obstruction as compared to the immunocompetent Tg+ and *Rag1*^{KO}/Tg+ juveniles (Fig. 7A–B). These data are inconsistent with our observation that the BALF from *Il2rg*^{KO}/Tg+ and *Il2rg*^{KO}/*Rag1*^{KO}/Tg+ juveniles had smaller and fewer mucus plugs as compared to immunocompetent Tg+ and *Rag1*^{KO}/Tg+ juveniles.

Immunohistochemical staining and gene expression analyses for two gel-forming mucins, MUB5B and MUC5AC were performed on lung sections. MUC5B immunostaining intensity was robust in immunocompetent WT and *Rag1*^{KO}/WT juveniles. In contrast, the *Il2rg*^{KO}/WT and *Il2rg*^{KO}/*Rag1*^{KO}/WT juveniles had reduced staining intensity (Supplemental Fig. 4A). Both immunocompetent Tg+ as well as *Rag1*^{KO}/Tg+ juveniles had robust MUC5B immunostaining of the airway epithelial cells and luminal contents (Fig. 7A). The intracellular staining for MUC5B was evident in *Il2rg*^{KO}/Tg+ and *Il2rg*^{KO}/*Rag1*^{KO}/Tg+ juveniles but was of lesser intensity as compared to immunocompetent Tg+ as well as *Rag1*^{KO}/Tg+ juveniles. Luminal contents in all the four Tg+ groups were intensely stained for MUC5B (Fig. 7A).

The *Muc5*b mRNA signatures were 1.23 ± 0.30, 1.42 ± 0.54, 2.35 ± 0.47, and 0.80 ± 0.12 -fold higher in immunocompetent WT, *Il2rg*^{KO}/WT, *Rag1*^{KO}/WT, and *Il2rg*^{KO}/*Rag1*^{KO}/WT juveniles, respectively. As compared to immunocompetent WT juveniles, the transcript levels for *Muc5*b were significantly elevated in the immunocompetent Tg+ (6.03 ± 1.16) and

Rag1^{KO}/Tg+ + (5.39 ± 1.19) juveniles (Fig. 7C). In contrast, the fold increase was significantly reduced in *Il2rg*^{KO}/Tg+ (3.62 ± 0.62) and *Il2rg*^{KO}/*Rag1*^{KO}/Tg+ (3.24 ± 0.56) juveniles (Fig. 7C).

As compared to immunocompetent WT juveniles, while MUC5AC immunostaining intensity was robust in *Rag1*^{KO}/WT, the *Il2rg*^{KO}/WT and *Il2rg*^{KO}/*Rag1*^{KO}/WT juveniles had reduced staining intensity (Supplemental Fig. 4B). Both immunocompetent Tg+ as well as *Rag1*^{KO}/Tg+ juveniles had robust MUC5AC immunostaining of the airway epithelial cells as well as luminal contents (Fig. 7A). In contrast, the intracellular as well as luminal immunostaining for MUC5AC in *Il2rg*^{KO}/Tg+ and *Il2rg*^{KO}/*Rag1*^{KO}/Tg+ juvenile was almost absent (Fig. 7A). Expression of *Muc5ac* gene was comparable between immunocompetent, *Il2rg*^{KO}, *Rag1*^{KO}, and *Il2rg*^{KO}/*Rag1*^{KO} juveniles on WT background (Fig 7 D). Among the four groups with Tg+ background, only *Rag1*^{KO}/Tg+ juveniles had significantly elevated levels of *Muc5ac* transcripts (Fig 7D).

Discussion:

Mucous cell metaplasia (MCM) and increased mucus production are *Th2*-associated responses (26–28) and interleukin 33 (IL-33) is a critical player in the manifestation of *Th2* responses (29, 30). Accordingly, we recently investigated the effect of IL-33 deficiency on MCM and mucus obstruction in *Scnn1b*-Tg+ (Tg+) mouse (9), a well-accepted mouse model that recapitulates multiple features of human muco-obstructive lung diseases (31). On the background of systemic IL-33 deficiency, the Tg+ juveniles were completely devoid of MCM, but the airway mucus obstruction persisted. In contrast to IL-33 sufficient Tg+ juveniles, the IL-33 deficient Tg+ juveniles had comparable gene expression levels of the two gel -forming mucins, i.e., *Muc5b* and *Muc5ac*, the BALF contents of secreted MUC5AC protein, but not MUC5B, was significantly reduced. Although our findings revealed the role of IL-33 in the MUC5AC contributions to mucus obstruction in Tg+ juveniles, the identity and role of cellular players that mediated MUC5B dominated mucus obstruction remained unclear.

Apart from *Th2*-dominated pathology, increased airway mucus production is also associated with inflammatory responses that are mediated through non-*Th2* cells or their products (10, 32, 33). Therefore, to complement our recent study, where *Th2* responses were blunted in IL-33-deficient Tg+ mice, we investigated mice in which *Th2* as well as non-*Th2* cells of the innate lymphoid and adaptive immune systems were modified as compared to their naïve states in WT and Tg+ mice. This study addresses a critical question, i.e., do the two major immune defense systems, innate lymphoid and adaptive, regulate mucous cell metaplasia (MCM) and muco-inflammatory responses of airway epithelial cells to airway surface liquid layer dehydration?

Like B- and T-lymphocytes of the adaptive immune system, the innate lymphoid cell (ILC) subsets originate from a common lymphoid precursor but lack antigen-specific receptors (34, 35). The transcriptional and functional machinery of ILCs mirrors that of adaptive immune cells (12, 34, 36). Accordingly, ILCs, i.e., ILC1, ILC2, ILC3, and NK cells represent amnestic equivalents of adaptive immune cells *Th1, Th2, Th17, and cytotoxic T*

cells, respectively (11–14). Because the development of ILC subtypes from a common lymphoid precursor requires signaling through the common gamma chain of the IL-2 receptor (IL2RG), the *Interleukin-2 receptor-gamma (Il2rg)* knockout mice (*Il2rg*^{KO}) lack ILCs but retain a limited number of T and B lymphocytes (15). On the other hand, due to the absence of *Recombination activating gene-1 (Rag1), Rag1* knockout mice (*Rag1*^{KO}) lack mature B- and T-lymphocytes of the adaptive immune system (16). The experimental design adopted in this study is unique in that direct comparisons between *Il2rg*^{KO}, *Rag1*^{KO}, and *Il2rg*^{KO}/*Rag1*^{KO} have been made in the context of Tg+ muco-inflammatory lung disease.

Our previous report on the longitudinal gene expression analyses in Tg+ mice at four disease-relevant age points revealed predominantly *Th1*-associated M1-like macrophage activation at PND3 and *Th2*-associated M2-like macrophage activation at PND42 (7). At PND10, the macrophage activation relevant gene signatures reflected mixed activation responses, i.e., markers of both M1-like and M2-like macrophage activation were observed (7). Therefore, we performed flow cytometry to characterize the immune cells present in the lungs of 10 days old WT and Tg+ neonates. These analyses revealed that in contrast to the WT lungs, the Tg+ lungs had: 1) increased proportions of ILC2 and *Th2* cells (Fig. 1A–B), 2) reduced proportions of ILC1 and *Th1* cells, 3) increased proportion of *Th1/Th2* hybrid cells, and 4) comparable proportions of ILC3 and *Th17* cells. These data suggest ILC2/*Th2* predominated airspace pathology in the 10-days old Tg+ pups which, most likely, progresses towards a more robust ILC2/*Th2* pathology later in life as evident by robust M2-like macrophage activation in adult Tg+ mice (7). This is also supported by upregulated expression of M2-like macrophage activation relevant gene signatures, including *Mmp12, Retnla, and Chi3l4*, in immunosufficient Tg+ juveniles (Fig. 5).

During early postnatal life, mice are prone to aspiration of oropharyngeal secretions that contain residential microbes, that are generally cleared by effective MCC and immune defense mechanisms (6). This bacterial burden was significantly elevated in 6–7day old WT neonates with ILCs deficiency, suggesting beneficial roles of various subsets of ILCs in bacterial clearance. Since IL-33 is a critical factor in the development of ILC2s (37) and IL-33 deficient WT mice did not exhibit similar elevations in bacterial burden (9), it is plausible that the absence of non-ILC2s (ILC1, 3, or NK cells) results in increased bacterial burden in *Il2rg*^{KO}/WT neonates. Thymic stromal lymphopoietin (TSLP)-driven, i.e., IL-33 independent, ILC2 development has been reported (38) which suggests a possibility that these novel ILC2 subsets might contribute to the bacterial clearance in Tg+ mice. Therefore, the exact identity of the ILC subsets in bacterial clearance in Tg+ mice remains to be tested.

Interestingly, as compared to immunosufficient WT mice, while the loss of innate immune lymphoid system exacerbated bacterial burden, the concomitant ablation of the adaptive immune system significantly compensated for the exacerbated bacterial burden that was caused by loss of innate lymphoid system (Fig. 2). These data suggest that the cellular or humoral components of the adaptive immune system have suppressive effects on the innate lymphoid system-mediated bacterial clearance mechanisms. However, the mechanistic interactions between these two arms of the immune system and their influence on bacterial clearance potential of phagocytes, i.e., macrophages and neutrophils, remain unexplored.

Interleukin 10 (IL-10) is a known immunosuppressive and anti-inflammatory cytokine (23, 39, 40). Among others, the cells of the adaptive immune system, including *T-helper* and *T-regulatory* cells (*Treg*), are the known producers of IL-10 (22, 24, 25). Reduced levels of IL-10 in the BALF from four groups deficient in adaptive immune system (Fig. 3A) suggest that the cells of the adaptive immunity are the primary source of IL-10 levels in the BALF. Based on the association between the magnitude of CFU and the levels of IL-10 in BALF, we hypothesized that IL-10 may suppress the functioning of cellular players that are essential for bacterial clearance. Therefore, we utilized an intranasal aspiration model to introduce residential oropharyngeal microbes in the lungs of *Il2rg*^{KO}/*Rag1*^{KO} /WT pups that were either treated simultaneously with IL-10 or PBS (vehicle) (Fig. 3B). Interestingly, as compared to PBS-treated *Il2rg*^{KO}/*Rag1*^{KO}/WT pups, *Il2rg*^{KO}/*Rag1*^{KO}/WT pups that received IL-10 exhibited greater bacterial burden (Fig. 3C) and reduced macrophage activation (Fig. 3G–J). The critical role played by macrophages in bacterial clearance in WT as well as Tg+ neonates has been previously reported (17). Consistent with this report, our current study also suggests that airspace macrophages constitute a major antibacterial defense system in WT and immunodeficient mice.

While this study suggests immunosuppressive effect of IL-10 on macrophages as one plausible reason for the greater susceptibility to bacterial infections in *Il2rg*^{KO}/WT pups, further investigation of the role of IL-10 in modulating bacterial clearance responses is awaited. Two intriguing questions remain unanswered: 1) Does IL-10 affect the composition of bacterial species in Tg+ mice, and 2) Whether the IL-10 mediated immunosuppression of other target cells, including ILCs (21), dendritic cells (41), and neutrophils (20), also contribute to the poor bacterial clearance response in *Il2rg*^{KO}/WT pups. Future studies employing approaches such as pharmacological inhibition or genetic ablation of IL-10 in Tg + mice and the use of IL-10 reporter strains might address these critical questions.

The spontaneous bacterial infections are consistently present in the Tg+ neonates, but these infections are cleared as the neonates mature (6), a trend that was also observed in this study. Previous reports speculated that the clearance of bacterial infection in adulthood is most likely a consequence of age-associated maturation of the immune system (6, 42). Our data suggest that the presence of an intact innate lymphoid system, but not the adaptive immune system, is crucial for the improved bacterial clearance in the Tg+ juveniles. Indeed, as seen in *Rag1*^{KO}/WT neonates, the loss of adaptive immune system in Tg+ neonates and juveniles appeared to promote bacterial clearance.

Mucus plugs provide a hypoxic but fertile microenvironment, a suitable niche for the colonization of microaerophilic bacterial species (43, 44). Accordingly, the degree of bacterial burden of microaerophilic species was expected to be lower in mice strain with reduced mucus obstruction, e.g., *Il2rg*^{KO}/*Rag1*^{KO}/Tg+ as compared to *Rag1*^{KO}/Tg+ juveniles (Fig. 3B). Contrary to this expectation, both *Il2rg*^{KO}/*Rag1*^{KO}/Tg+ and *Rag1*^{KO}/Tg + juveniles had comparable bacterial burden indicating that the reduced mucus obstruction was not beneficial to the former group. These findings point towards a possibility that the bacterial burden in the Tg+ mice persisted as a result of poor phagocytic capabilities of phagocytes rather than exaggerated mucus obstruction. This possibility was also suggested in a previous report on Tg+ mice where partial depletion of macrophages severely

compromised bacterial clearance leading to lethal pneumonia in a significant proportion of neonates (17). On the other hand, the magnitude of bacterial burden was poorly associated with the degree of mucus obstruction. One plausible reason for this may be that while mucus plugs provide a suitable niche for bacterial growth, the buildup of MUC5B, an antibacterial defense protein (45) and the primary contributor to mucus plugging in the Tg+ mice (46), could also counter bacterial growth within the mucus plugs.

We recently demonstrated that IL-33 is essential for the recruitment of eosinophils into the airspaces of Tg+ juveniles (9). IL-33 binds to various cell types, including naïve ILCs and other non-ILC cells (47) that bear its receptor (ST2), to mediate eosinophil recruitment in Tg + juveniles. Our current data suggest a dichotomy between the innate lymphoid and the adaptive immune systems in mediating eosinophil recruitment into the Tg+ airspaces. Similar to IL-33 deficient Tg+ juveniles, the *Il2rg*^{KO}/Tg+ juveniles lack airspace eosinophils suggesting that, most likely, the ILCs, in particular ILC2, respond to IL-33 during eosinophilic recruitment to Tg+ airspaces. Conversely, *Rag1*^{KO}/Tg+ juveniles did not exhibit impaired eosinophil recruitment, suggesting, in the absence of adaptive immune cells, ILCs can independently respond to IL-33 during eosinophilic recruitment to Tg+ airspaces. Of note, following the trend of eosinophil recruitment, IL-5, a key eosinophil chemoattractant, was absent in *Il2rg*^{KO}/Tg+ but not in *Rag1*^{KO}/Tg+ juveniles. Here, whereas we have demonstrated that adaptive immune cells are dispensable in the recruitment of eosinophils, the identity of indispensable cells other than ILCs, if any, in eosinophilic recruitment remains elusive.

The Tg+ mice exhibit elevated gene expression for the markers of *Th2* inflammation, including *Slc26a4* (*Pendrin*), *Clca1/3 (Gob5)*, *Retnla* (*Fizz1*), and *Chi3l4* (*YM2*) (7–9). The expression levels of each of these markers were comparable between immunocompetent Tg+ and *Rag1*^{KO}/Tg+ juveniles, suggesting that adaptive immune system does not contribute to the *Th2* inflammatory responses in Tg+ juveniles. In the absence of innate lymphoid cells, the expression levels of all the four markers were suppressed to significantly lower levels. Interestingly, although significantly lower than immunocompetent Tg+, the *Il2rg*^{KO}/ *Rag1*^{KO}/Tg+ juveniles had *Slc26a4* and *Chi3l4* expression above basal levels, suggesting the involvement of additional mechanisms in their upregulated expression in Tg+ lungs.

A significant increase in the proportion of airway mucous cells, i.e. mucous cell metaplasia, is observed in the WT juveniles that wanes towards adulthood (18). While this feature was consistently observed in immunocompetent WT and *Rag1*^{KO}/WT juveniles, the *Il2rg*^{KO}/WT and *Il2rg*^{KO}/*Rag1*^{KO}/WT groups were virtually devoid of AB-PAS^{+} airway mucous cells. As compared to WT counterparts, while the immunocompetent Tg+ and *Rag1*^{KO}/Tg+ juveniles had a significantly higher proportion of mucous cells, the *Il2rg*^{KO}/Tg+ and *Il2rg*^{KO}/ *Rag1*^{KO}/Tg+ juveniles remained devoid of AB-PAS^{+} mucous cells. Along similar lines, the gene expression levels for MCM-relevant genes, i.e., *Agr2, Tff2,* and *Gata3* trended lower in *Il2rg*^{KO}/WT and *Il2rg*^{KO}/*Rag1*^{KO}/WT juveniles as compared to immunocompetent WT or *Rag1*^{KO}/WT juveniles. Further, the *Il2rg*^{KO}/Tg+ and *Il2rg*^{KO}/*Rag1*^{KO}/Tg+ juveniles had significantly lower levels of *Spdef, Agr2, Tff2,* and *Gata3* transcripts compared to immunocompetent Tg+ mice. These data are consistent with a previous report in which the ablation of ILCs resulted in diminished goblet cell hyperplasia in helminth-infected mice

(32). These data suggest that the expression level of MCM-relevant genes and the intracellular accumulation of glycosylated mucins in the airway epithelial cells is regulated by innate lymphoid cells. These outcomes were not mitigated in the absence of adaptive immune cells.

MCM responses are often associated with increase in mucus obstruction (48–51). However, despite the presence of a significant number of AB-PAS^{+} mucous cells (~30–33 cells/mm of basement membrane) in immunocompetent WT and *Rag1*^{KO}/WT juveniles, no mucus obstruction was evident (Fig. 6A). Interestingly, with just a two-fold increase in the number of AB-PAS^{+} mucous cells (~50–60 cells/mm of basement membrane) in immunocompetent Tg+ and *Rag1*^{KO}/Tg+ juveniles, mucus obstruction was clearly evident in the airways (Fig. 6A). On the other hand, despite complete loss of AB-PAS^{+} mucous cells in *Il2rg*^{KO}/Tg+ juveniles, mucus obstruction persisted. Only *Il2rg*^{KO}/*Rag1*^{KO}/Tg+ mice had significant reduction in mucus obstruction, which was associated with reduction in *Muc5b* gene expression and MUC5B-specific staining of epithelial and luminal mucopolysaccharides (Fig. 7). As evident by studies on MUC5AC- and MUC5B-deficient mice crossed with Tg+ mice, ablation of MUC5AC was not associated with a reduction in mucus obstruction whereas MUC5B was associated with ~50% reduction in mucus obstruction (46). Therefore, the reduction in mucus obstruction observed in the *Il2rg*^{KO}/*Rag1*^{KO}/Tg+ juveniles could reflect in part the reduction in MUC5B expression, rather than MUC5AC expression.

Lung ILC2s are known to produce *Th2* cytokines in diverse disease models including allergic asthma and helminths infections (52–54). ILC2s were demonstrated as the primary source of IL-5 and IL-13 that were able to induce airway inflammation and airway hyperresponsiveness in murine models of asthma (46, 47). ILC2s from human asthmatics have also been identified as the producers of both, IL-5 and IL-13 (55, 56). The contribution of ILC2s towards IL-4 production however remains controversial, although, a recent study reported IL-4 production by IL-25 responsive pulmonary ILC2s (54). Based on our findings that imply a strong association between ILCs deficiency and reduced levels of Th2 cytokines (Fig. 4J, 5A–C), it remains unclear whether ILC2s are the direct source of *Th2* cytokines, i.e. IL-4, IL-5, and IL-13, in the Tg+ mice. This is because the deficiency of *Il2rg* not only disrupts ILCs development (15), but also affects other signaling pathways that require gamma chain, e.g., Type I IL-4 Receptor α, (heterodimeric Type 1 IL4Rα receptor complex that contains common gamma chain) (57). Therefore, the reduced levels of *Th2* cytokines in *Il2rg*^{KO}/Tg+ juveniles might be an upshot of disrupted signaling pathways prevalent in non-ILCs. Both, IL-4 and IL-5, were found to be reduced in our previous study where IL-33 was depleted in Tg+ mice indicating that IL-33 regulated ILC2s might act as a source of these cytokines in these mice (9). Of note, IL-33 knockout mice are also known to exhibit TSLP-regulated expansion of IL13 expressing ILC2s (38), but these ILCs, if present, were not responsible for the maintenance of IL-4/IL-5 levels in IL-33 deficient Tg+ mice in our study. Despite these evidence, further studies pinpointing the source of *Th2* cytokines in *Tg+* mice are warranted in refined experimental models with deficiency of individual ILC subsets.

In conclusion, this study revealed interesting contributions of the innate lymphoid and adaptive immune systems to the pathogenesis of Tg+ lung disease (Fig. 8). First, the innate lymphoid system is beneficial in the bacterial clearance in WT and Tg+ mice. Second, the

ablation of the adaptive immune system promotes macrophage activation and likely facilitates bacterial clearance. Third, innate lymphoid cells, not adaptive immune cells, are essential for the recruitment of eosinophils to the Tg+ airspaces. Fourth, the innate lymphoid system, but not the adaptive immune system, mediates *Th2* responses in the Tg+ airspaces. Fifth, mucous cell metaplasia is abolished in the absence of innate lymphoid cells. Finally, the ablation of innate lymphoid cells suppresses the expression of gel-forming mucins but not mucus obstruction. Collectively, these findings suggest critical roles of the innate lymphoid system in bacterial clearance, mucous cell metaplasia, and mucin production and that these responses are independent of the adaptive immune system.

Supplementary Material

Refer to Web version on PubMed Central for supplementary material.

Acknowledgments

We thank Dr. Camille Ehre (University of North Carolina at Chapel Hill) for providing MUC5B and MUC5AC antibodies. We thank Sherry Ring for histological tissue processing and Thaya Stoufflet for assistance with multiplex cytokine assays.

Funding: This work was supported by National Institute of General Medical Sciences Grant 5P30GM110760 (Pilot Project Funding), National Institute of General Medical Sciences Grant P20GM130555 (to Y.S.), and National Institute of Environmental Health Sciences Grant R01ES030125 (to Y.S.).

References

1. Knowles MR, and Boucher RC 2002 Mucus clearance as a primary innate defense mechanism for mammalian airways. J Clin Invest 109: 571–577. [PubMed: 11877463]
2. Boucher RC 2007 Airway surface dehydration in cystic fibrosis: pathogenesis and therapy. Annu Rev Med 58: 157–170. [PubMed: 17217330]
3. Fahy JV, and Dickey BF 2010 Airway mucus function and dysfunction. N Engl J Med 363: 2233–2247. [PubMed: 21121836]
4. Mall M, Grubb BR, Harkema JR, O'Neal WK, and Boucher RC 2004 Increased airway epithelial Na + absorption produces cystic fibrosis-like lung disease in mice. Nat Med 10: 487–493. [PubMed: 15077107]
5. Mall MA, Harkema JR, Trojanek JB, Treis D, Livraghi A, Schubert S, Zhou Z, Kreda SM, Tilley SL, Hudson EJ, O'Neal WK, and Boucher RC 2008 Development of chronic bronchitis and emphysema in beta-epithelial Na+ channel-overexpressing mice. Am J Respir Crit Care Med 177: 730–742. [PubMed: 18079494]
6. Livraghi-Butrico A, Kelly EJ, Klem ER, Dang H, Wolfgang MC, Boucher RC, Randell SH, and O'Neal WK 2012 Mucus clearance, MyD88-dependent and MyD88-independent immunity modulate lung susceptibility to spontaneous bacterial infection and inflammation. Mucosal Immunol 5: 397–408. [PubMed: 22419116]
7. Saini Y, Dang H, Livraghi-Butrico A, Kelly EJ, Jones LC, O'Neal WK, and Boucher RC 2014 Gene expression in whole lung and pulmonary macrophages reflects the dynamic pathology associated with airway surface dehydration. BMC Genomics 15: 726. [PubMed: 25204199]
8. Lewis BW, Sultana R, Sharma R, Noel A, Langohr I, Patial S, Penn AL, and Saini Y. 2017 Early Postnatal Secondhand Smoke Exposure Disrupts Bacterial Clearance and Abolishes Immune Responses in Muco-Obstructive Lung Disease. J Immunol 199: 1170–1183. [PubMed: 28667160]
9. Lewis BW, Vo T, Choudhary I, Kidder A, Bathula C, Ehre C, Wakamatsu N, Patial S, and Saini Y. 2020 Ablation of IL-33 Suppresses Th2 Responses but Is Accompanied by Sustained Mucus Obstruction in the Scnn1b Transgenic Mouse Model. J Immunol 204: 1650–1660. [PubMed: 32060135]

10. Cohn L, Homer RJ, Niu N, and Bottomly K. 1999 T helper 1 cells and interferon gamma regulate allergic airway inflammation and mucus production. J Exp Med 190: 1309–1318. [PubMed: 10544202]
11. Moro K, Yamada T, Tanabe M, Takeuchi T, Ikawa T, Kawamoto H, Furusawa J, Ohtani M, Fujii H, and Koyasu S. 2010 Innate production of T(H)2 cytokines by adipose tissue-associated c-Kit(+)Sca-1(+) lymphoid cells. Nature 463: 540–544. [PubMed: 20023630]
12. Shih HY, Sciume G, Poholek AC, Vahedi G, Hirahara K, Villarino AV, Bonelli M, Bosselut R, Kanno Y, Muljo SA, and O'Shea JJ 2014 Transcriptional and epigenetic networks of helper T and innate lymphoid cells. Immunol Rev 261: 23–49. [PubMed: 25123275]
13. Spits H, and Di Santo JP 2011 The expanding family of innate lymphoid cells: regulators and effectors of immunity and tissue remodeling. Nat Immunol 12: 21–27. [PubMed: 21113163]
14. Spits H, Artis D, Colonna M, Diefenbach A, Di Santo JP, Eberl G, Koyasu S, Locksley RM, McKenzie AN, Mebius RE, Powrie F, and Vivier E. 2013 Innate lymphoid cells--a proposal for uniform nomenclature. Nat Rev Immunol 13: 145–149. [PubMed: 23348417]
15. Cao X, Shores EW, Hu-Li J, Anver MR, Kelsall BL, Russell SM, Drago J, Noguchi M, Grinberg A, Bloom ET, and et al. 1995 Defective lymphoid development in mice lacking expression of the common cytokine receptor gamma chain. Immunity 2: 223–238. [PubMed: 7697543]
16. Mombaerts P, Iacomini J, Johnson RS, Herrup K, Tonegawa S, and Papaioannou VE 1992 RAG-1-deficient mice have no mature B and T lymphocytes. Cell 68: 869–877. [PubMed: 1547488]
17. Saini Y, Wilkinson KJ, Terrell KA, Burns KA, Livraghi-Butrico A, Doerschuk CM, O'Neal WK, and Boucher RC 2016 Neonatal Pulmonary Macrophage Depletion Coupled to Defective Mucus Clearance Increases Susceptibility to Pneumonia and Alters Pulmonary Immune Responses. Am J Respir Cell Mol Biol 54: 210–221. [PubMed: 26121027]
18. Livraghi A, Grubb BR, Hudson EJ, Wilkinson KJ, Sheehan JK, Mall MA, O'Neal WK, Boucher RC, and Randell SH 2009 Airway and lung pathology due to mucosal surface dehydration in {beta}-epithelial Na+ channel-overexpressing mice: role of TNF-{alpha} and IL-4R{alpha} signaling, influence of neonatal development, and limited efficacy of glucocorticoid treatment. J Immunol 182: 4357–4367. [PubMed: 19299736]
19. Schneider CA, Rasband WS, and Eliceiri KW 2012 NIH Image to ImageJ: 25 years of image analysis. Nat Methods 9: 671–675. [PubMed: 22930834]
20. Sun L, Guo RF, Newstead MW, Standiford TJ, Macariola DR, and Shanley TP 2009 Effect of IL-10 on neutrophil recruitment and survival after Pseudomonas aeruginosa challenge. Am J Respir Cell Mol Biol 41: 76–84. [PubMed: 19097982]
21. Ogasawara N, Poposki JA, Klingler AI, Tan BK, Weibman AR, Hulse KE, Stevens WW, Peters AT, Grammer LC, Schleimer RP, Welch KC, Smith SS, Conley DB, Raviv JR, Soroosh P, Akbari O, Himi T, Kern RC, and Kato A. 2018 IL-10, TGF-beta, and glucocorticoid prevent the production of type 2 cytokines in human group 2 innate lymphoid cells. J Allergy Clin Immunol 141: 1147–1151 e1148.
22. Fiorentino DF, Bond MW, and Mosmann TR 1989 Two types of mouse T helper cell. IV. Th2 clones secrete a factor that inhibits cytokine production by Th1 clones. J Exp Med 170: 2081–2095. [PubMed: 2531194]
23. Fiorentino DF, Zlotnik A, Mosmann TR, Howard M, and O'Garra A. 2016 Pillars Article: IL-10 Inhibits Cytokine Production by Activated Macrophages. J. Immunol 1991 147: 3815–3822. J Immunol 197: 1539–1546.
24. Ouyang W, Rutz S, Crellin NK, Valdez PA, and Hymowitz SG 2011 Regulation and functions of the IL-10 family of cytokines in inflammation and disease. Annu Rev Immunol 29: 71–109. [PubMed: 21166540]
25. Moore KW, de Waal Malefyt R, Coffman RL, and O'Garra A. 2001 Interleukin-10 and the interleukin-10 receptor. Annu Rev Immunol 19: 683–765. [PubMed: 11244051]
26. Dabbagh K, Takeyama K, Lee HM, Ueki IF, Lausier JA, and Nadel JA 1999 IL-4 induces mucin gene expression and goblet cell metaplasia in vitro and in vivo. J Immunol 162: 6233–6237. [PubMed: 10229869]
27. McKenzie GJ, Bancroft A, Grencis RK, and McKenzie AN 1998 A distinct role for interleukin-13 in Th2-cell-mediated immune responses. Curr Biol 8: 339–342. [PubMed: 9512421]

28. Komai M, Tanaka H, Masuda T, Nagao K, Ishizaki M, Sawada M, and Nagai H. 2003 Role of Th2 responses in the development of allergen-induced airway remodelling in a murine model of allergic asthma. Br J Pharmacol 138: 912–920. [PubMed: 12642393]
29. Kondo Y, Yoshimoto T, Yasuda K, Futatsugi-Yumikura S, Morimoto M, Hayashi N, Hoshino T, Fujimoto J, and Nakanishi K. 2008 Administration of IL-33 induces airway hyperresponsiveness and goblet cell hyperplasia in the lungs in the absence of adaptive immune system. Int Immunol 20: 791–800. [PubMed: 18448455]
30. Eiwegger T, and Akdis CA 2011 IL-33 links tissue cells, dendritic cells and Th2 cell development in a mouse model of asthma. Eur J Immunol 41: 1535–1538. [PubMed: 21618506]
31. Boucher RC 2019 Muco-Obstructive Lung Diseases. N Engl J Med 380: 1941–1953. [PubMed: 31091375]
32. Campbell L, Hepworth MR, Whittingham-Dowd J, Thompson S, Bancroft AJ, Hayes KS, Shaw TN, Dickey BF, Flamar AL, Artis D, Schwartz DA, Evans CM, Roberts IS, Thornton DJ, and Grencis RK 2019 ILC2s mediate systemic innate protection by priming mucus production at distal mucosal sites. J Exp Med 216: 2714–2723. [PubMed: 31582416]
33. Chen Y, Thai P, Zhao YH, Ho YS, DeSouza MM, and Wu R. 2003 Stimulation of airway mucin gene expression by interleukin (IL)-17 through IL-6 paracrine/autocrine loop. J Biol Chem 278: 17036–17043.
34. Vivier E, van de Pavert SA, Cooper MD, and Belz GT. 2016 The evolution of innate lymphoid cells. Nat Immunol 17: 790–794. [PubMed: 27328009]
35. Eberl G, Colonna M, Di Santo JP, and McKenzie AN 2015 Innate lymphoid cells. Innate lymphoid cells: a new paradigm in immunology. Science 348: aaa6566.
36. Sciume G, Shih HY, Mikami Y, and O'Shea JJ 2017 Epigenomic Views of Innate Lymphoid Cells. Front Immunol 8: 1579. [PubMed: 29250060]
37. Schmitz J, Owyang A, Oldham E, Song Y, Murphy E, McClanahan TK, Zurawski G, Moshrefi M, Qin J, Li X, Gorman DM, Bazan JF, and Kastelein RA 2005 IL-33, an interleukin-1-like cytokine that signals via the IL-1 receptor-related protein ST2 and induces T helper type 2-associated cytokines. Immunity 23: 479–490. [PubMed: 16286016]
38. Verma M, Liu S, Michalec L, Sripada A, Gorska MM, and Alam R. 2018 Experimental asthma persists in IL-33 receptor knockout mice because of the emergence of thymic stromal lymphopoietin-driven IL-9(+) and IL-13(+) type 2 innate lymphoid cell subpopulations. J Allergy Clin Immunol 142: 793–803 e798.
39. Taga K, and Tosato G. 1992 IL-10 inhibits human T cell proliferation and IL-2 production. J Immunol 148: 1143–1148. [PubMed: 1737931]
40. Fiorentino DF, Zlotnik A, Vieira P, Mosmann TR, Howard M, Moore KW, and O'Garra A. 1991 IL-10 acts on the antigen-presenting cell to inhibit cytokine production by Th1 cells. J Immunol 146: 3444–3451. [PubMed: 1827484]
41. Mittal SK, Cho KJ, Ishido S, and Roche PA 2015 IL-10 mediated immunosuppression: March-I induction regulates antigen presentation by macrophages but not dendritic cells. J Biol Chem 290: 27158–27167.
42. Saini Y, Lewis BW, Yu D, Dang H, Livraghi-Butrico A, Del Piero F, O'Neal WK, and Boucher RC 2018 Effect of LysM+ macrophage depletion on lung pathology in mice with chronic bronchitis. Physiol Rep 6: e13677.
43. Randell SH, Boucher RC, and G. University of North Carolina Virtual Lung. 2006 Effective mucus clearance is essential for respiratory health. Am J Respir Cell Mol Biol 35: 20–28. [PubMed: 16528010]
44. Worlitzsch D, Tarran R, Ulrich M, Schwab U, Cekici A, Meyer KC, Birrer P, Bellon G, Berger J, Weiss T, Botzenhart K, Yankaskas JR, Randell S, Boucher RC, and Doring G. 2002 Effects of reduced mucus oxygen concentration in airway Pseudomonas infections of cystic fibrosis patients. J Clin Invest 109: 317–325. [PubMed: 11827991]
45. Roy MG, Livraghi-Butrico A, Fletcher AA, McElwee MM, Evans SE, Boerner RM, Alexander SN, Bellinghausen LK, Song AS, Petrova YM, Tuvim MJ, Adachi R, Romo I, Bordt AS, Bowden MG, Sisson JH, Woodruff PG, Thornton DJ, Rousseau K, De la Garza MM, Moghaddam SJ, Karmouty-Quintana H, Blackburn MR, Drouin SM, Davis CW, Terrell KA, Grubb BR, O'Neal

WK, Flores SC, Cota-Gomez A, Lozupone CA, Donnelly JM, Watson AM, Hennessy CE, Keith RC, Yang IV, Barthel L, Henson PM, Janssen WJ, Schwartz DA, Boucher RC, Dickey BF, and Evans CM 2014 Muc5b is required for airway defence. Nature 505: 412–416. [PubMed: 24317696]

46. Livraghi-Butrico A, Grubb BR, Wilkinson KJ, Volmer AS, Burns KA, Evans CM, O'Neal WK, and Boucher RC 2017 Contribution of mucus concentration and secreted mucins Muc5ac and Muc5b to the pathogenesis of muco-obstructive lung disease. Mucosal Immunol 10: 395–407. [PubMed: 27435107]
47. Griesenauer B, and Paczesny S. 2017 The ST2/IL-33 Axis in Immune Cells during Inflammatory Diseases. Front Immunol 8: 475. [PubMed: 28484466]
48. Whitsett JA 2018 Airway Epithelial Differentiation and Mucociliary Clearance. Ann Am Thorac Soc 15: S143–S148. [PubMed: 30431340]
49. Mall MA 2016 Unplugging Mucus in Cystic Fibrosis and Chronic Obstructive Pulmonary Disease. Ann Am Thorac Soc 13 Suppl 2: S177–185. [PubMed: 27115954]
50. Ma J, Rubin BK, and Voynow JA 2018 Mucins, Mucus, and Goblet Cells. Chest 154: 169–176. [PubMed: 29170036]
51. Jaramillo AM, Azzegagh Z, Tuvim MJ, and Dickey BF 2018 Airway Mucin Secretion. Ann Am Thorac Soc 15: S164–S170. [PubMed: 30431339]
52. Kim HY, Chang YJ, Subramanian S, Lee HH, Albacker LA, Matangkasombut P, Savage PB, McKenzie AN, Smith DE, Rottman JB, DeKruyff RH, and Umetsu DT 2012 Innate lymphoid cells responding to IL-33 mediate airway hyperreactivity independently of adaptive immunity. J Allergy Clin Immunol 129: 216–227 e211–216.
53. Bartemes KR, Iijima K, Kobayashi T, Kephart GM, McKenzie AN, and Kita H. 2012 IL-33-responsive lineage- CD25+ CD44(hi) lymphoid cells mediate innate type 2 immunity and allergic inflammation in the lungs. J Immunol 188: 1503–1513. [PubMed: 22198948]
54. Miller MM, Patel PS, Bao K, Danhorn T, O'Connor BP, and Reinhardt RL 2020 BATF acts as an essential regulator of IL-25-responsive migratory ILC2 cell fate and function. Sci Immunol 5.
55. Smith SG, Chen R, Kjarsgaard M, Huang C, Oliveria JP, O'Byrne PM, Gauvreau GM, Boulet LP, Lemiere C, Martin J, Nair P, and Sehmi R. 2016 Increased numbers of activated group 2 innate lymphoid cells in the airways of patients with severe asthma and persistent airway eosinophilia. J Allergy Clin Immunol 137: 75–86 e78.
56. Chen R, Smith SG, Salter B, El-Gammal A, Oliveria JP, Obminski C, Watson R, O'Byrne PM, Gauvreau GM, and Sehmi R. 2017 Allergen-induced Increases in Sputum Levels of Group 2 Innate Lymphoid Cells in Subjects with Asthma. Am J Respir Crit Care Med 196: 700–712. [PubMed: 28422515]
57. Junttila IS, Mizukami K, Dickensheets H, Meier-Schellersheim M, Yamane H, Donnelly RP, and Paul WE 2008 Tuning sensitivity to IL-4 and IL-13: differential expression of IL-4Ralpha, IL-13Ralpha1, and gammac regulates relative cytokine sensitivity. J Exp Med 205: 2595–2608. [PubMed: 18852293]

Key Points:

1: Innate lymphoid system promotes bacterial clearance from airspaces.

2: Innate lymphoid system mediates *Th2* responses in the Tg+ airspaces.

3: Ablation of Innate lymphoid system abolishes MCM in the Tg+ airspaces.

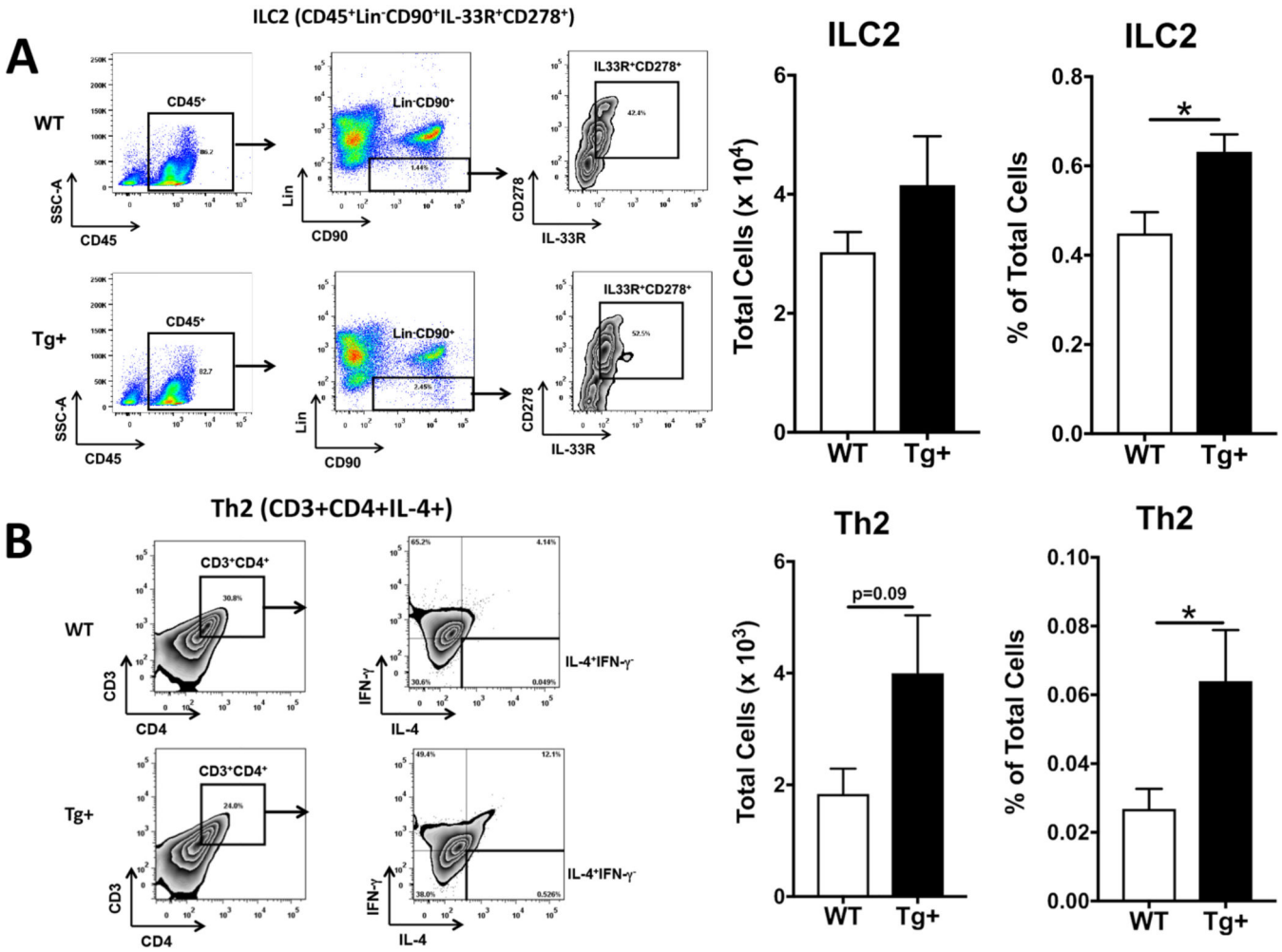

Figure 1: ILC2 and *Th2* cells are increased in the lungs of 10-day old Tg+ neonates.

Gating Strategy and representative scatter plots for flow cytometric characterization of ILC2 ($CD45^+Lin^-CD90^+IL\text{-}33R^+CD278^+$) in whole lung single cell suspension from WT (**A,** top panel) and Tg+ neonates (**A,** bottom panel) (n=5 of mice per group). Percent values in the scatter plots indicate the proportion of gated populations. Total counts for ILC2 (**A**, left bar graph) in whole lung single cell suspension from WT (white bar) and Tg+ (black bar) neonates (n= 5 of mice per group). Percentage of ILC2 (**A**, right bar graph) in whole lung single cell suspension from WT (white bar) and Tg+ (black bar) neonates. Error bars represent standard error of the mean (SEM). *p <0.05 analyzed by Student's t test. Gating Strategy and representative scatter plots for flow cytometric characterization of *Th2* cells ($CD3^+CD4^+IL\text{-}4^+$) in whole lung single cell suspension from WT (**B,** top panels) and Tg+ neonates (**B,** bottom panels) (n=5 of mice per group). Total counts for *Th2* (**B**, left bar graph) in whole lung single cell suspension from WT (white bar) and Tg+ (black bar) neonates (n=5 of mice per group). Percentage of *Th2* (**B,** right bar graph) whole lung single cell suspension from WT (white bar) and Tg+ (black bar) neonates. Scatter plots for the isotype controls of antibodies used in this figure are included in Supplemental Figure 1A.

Error bars represent SEM. *$p<0.05$ analyzed by Student's *t* test. WT, Wild Type; Tg+, *Scnn1b*-Tg+, ILC, Innate lymphoid cells; Th, T helper.

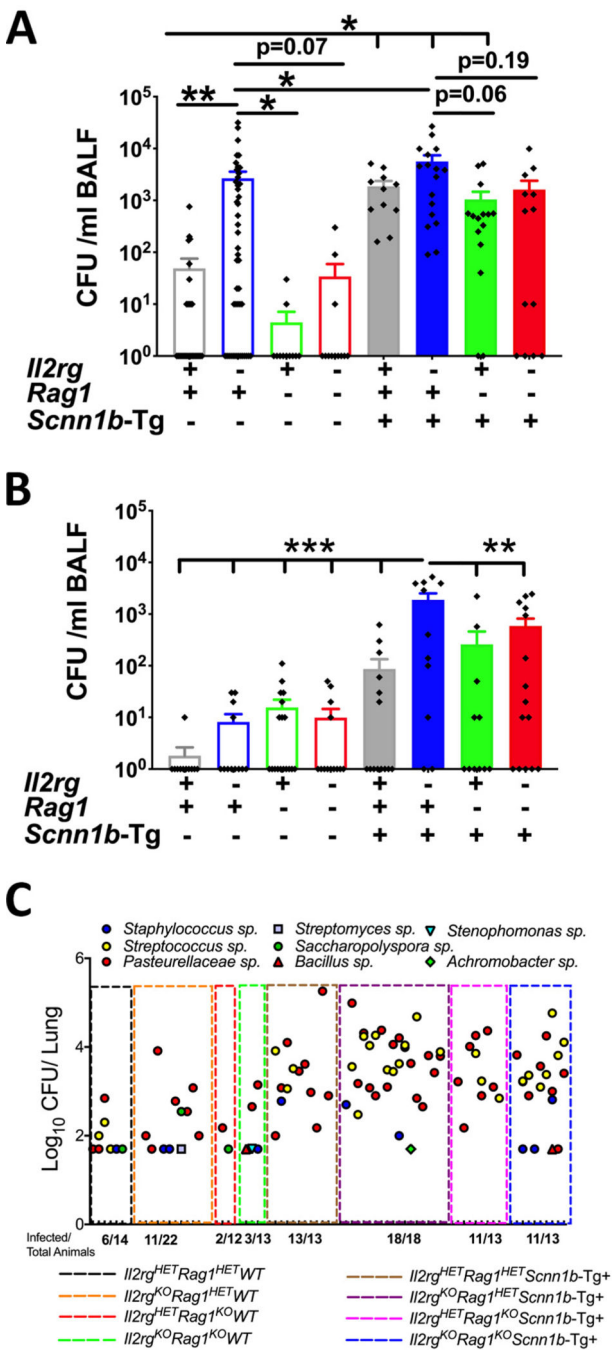

Figure 2: Ablation of innate lymphoid immune cells results in increased bacterial burden in WT and Tg+ mice.

(A) CFUs in BALF from immunocompetent WT (open gray bar, n=31), *Il2rg*^{KO}/WT (open blue bar, n=46), *Rag1*^{KO}/WT (open green bar, n=11), *Il2rg*^{KO}/*Rag1*^{KO}/WT (open red bar, n=12), immunocompetent Tg+ (solid gray bar, n=12), *Il2rg*^{KO}/Tg+ (solid blue bar, n=17), *Rag1*^{KO}/Tg+ (solid green bar, n=15), and *Il2rg*^{KO}/*Rag1*^{KO}/Tg+ (solid red bar, n=14) neonates. **(B)** CFUs in BALF from immunocompetent WT (open gray open bar, n=11), *Il2rg*^{KO}/WT (open blue open bar, n=12), *Rag1*^{KO}/WT (open green open bar, n=18), *Il2rg*^{KO}/

Rag1^{KO}/WT (open red open bar, n=13), immunocompetent Tg+ (open gray solid bar, n=14), *Il2rg*^{KO}/Tg+ (open blue solid bar, n=11), *Rag1*^{KO}/Tg+ (open green solid bar, n=11), and *Il2rg*^{KO}/*Rag1*^{KO}/Tg+ (open red solid bar, n=15) juveniles. The CFU values were log10-transformed with an offset of +1 (Log10+1 transformation). Error bars represent SEM. **(C)** Bacterial species identification using 16S gene sequencing on DNA isolated from cultured bacterial colonies. Non-parametric data (D'Agostino & Pearson test) were compared by the Kruskal-Wallis test followed by Dunn's post-test for multiple comparisons. Error bars represent SEM. *p<0.05; **p<0.01; ***p<0.001. BALF, Bronchoalveolar lavage fluid; CFU, Colony forming units, *Il2rg, Interleukin 2 receptor gamma*; *Rag1*, *Recombinase activating gene-1*.

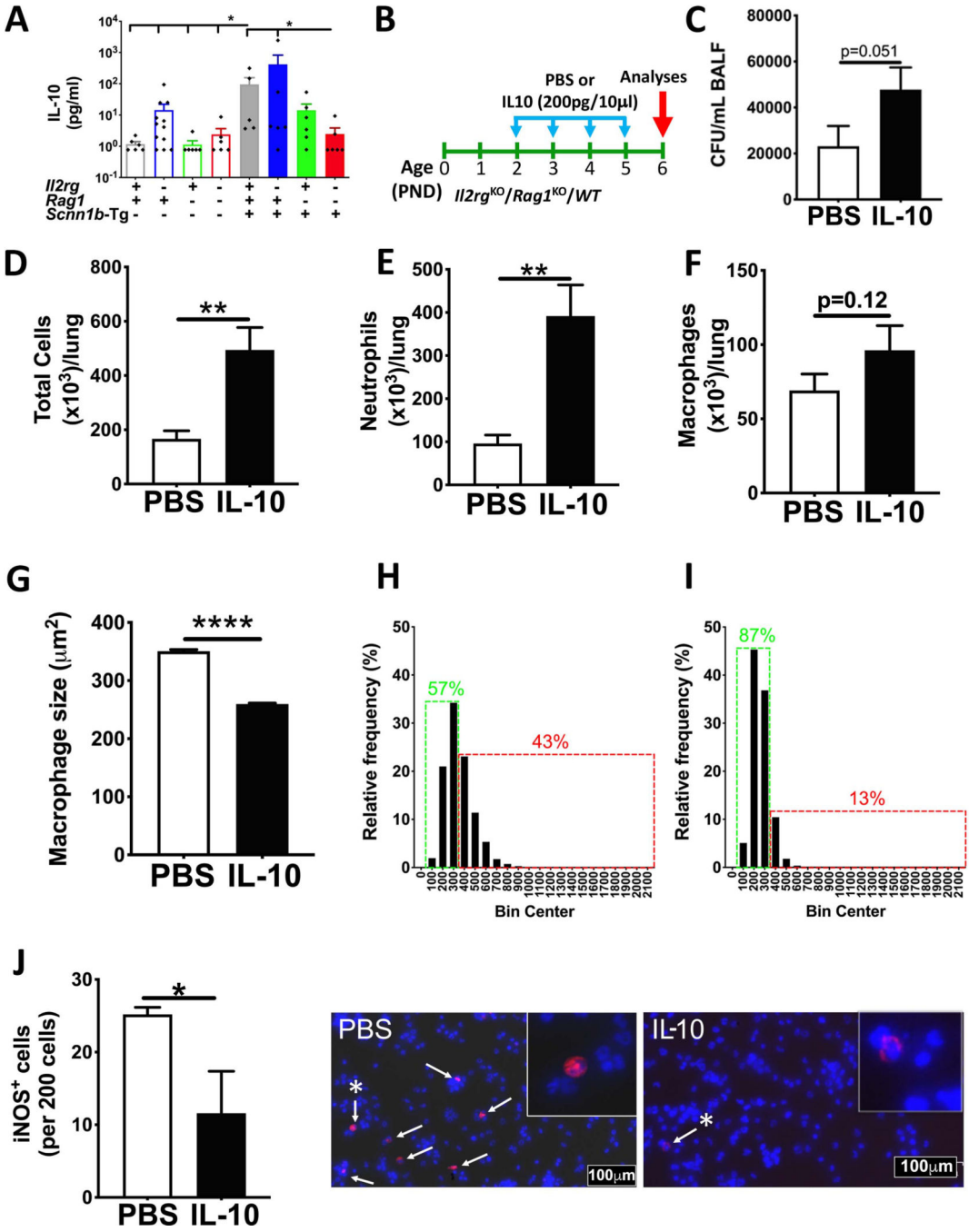

Figure 3: IL-10-mediates immunosuppression of proinflammatory macrophage activation.

BALF concentration of IL-10 **(A)** from 10 days old immunocompetent WT (open gray bar, n=6), *Il2rg*^{KO}/WT (open blue bar, n=12*)*, *Rag1*^{KO}/WT (open green bar, n=6), *Il2rg*^{KO}/*Rag1*^{KO}/WT (open red bar, n=6), immunocompetent Tg+ (solid gray bar, n=5), *Il2rg*^{KO}/Tg+ (solid blue bar, n=6), *Rag1*^{KO}/Tg+ (solid green bar, n=6), and *Il2rg*^{KO}/*Rag1*^{KO}/Tg+ (solid red bar, n=6) neonates. ANOVA followed by Tukey multiple comparison post-hoc test. * p <0.05. Error bars represent SEM. **(B)** Experimental design for IL-10 intranasal administration (PND 2–5) study on *Il2rg*^{KO}/*Rag1*^{KO}/WT neonates. CFU in BALF **(C)** from

6 days old PBS- (white bar, n=12) and IL-10-administered (black bar, n=14) *Il2rg*^{KO}/*Rag1*^{KO}/WT pups. Total number of cells **(D)**, neutrophils **(E)**, and macrophages **(F)** harvested in BALF from PBS- (white bar, n=12) and IL-10-administered (black bar, n=14) *Il2rg*^{KO}/*Rag1*^{KO}/WT pups. **(G)** Quantification of surface area of BALF macrophages from PBS- (white bar, n=5) and IL-10-administered (black bar, n=5) *Il2rg*^{KO}/*Rag1*^{KO}/WT pups. Macrophage size distribution of BALF macrophages from PBS- (n=5) **(H)** and IL-10-administered (n=5) **(I)** *Il2rg*^{KO}/*Rag1*^{KO}/WT pups. Total number of iNOS positive BALF macrophages from PBS- (white bar, n=3) and IL-10-administered (black bar, n=3) *Il2rg*^{KO}/*Rag1*^{KO}/WT pups. Representative images from immunostained cytospins for iNOS (white arrows, red) and nuclear staining (blue, DNA staining) in PBS- (**J**, left photomicrograph) and IL-10-administered pups (**J**, right photomicrograph). High resolution image of iNOS positive cells (asterisk-bearing white arrow) are shown as inset. Error bars represent SEM. *p<0.05; **p<0.01; ****p<0.0001; using Student's t-test. IL-10, Interleukin-10.

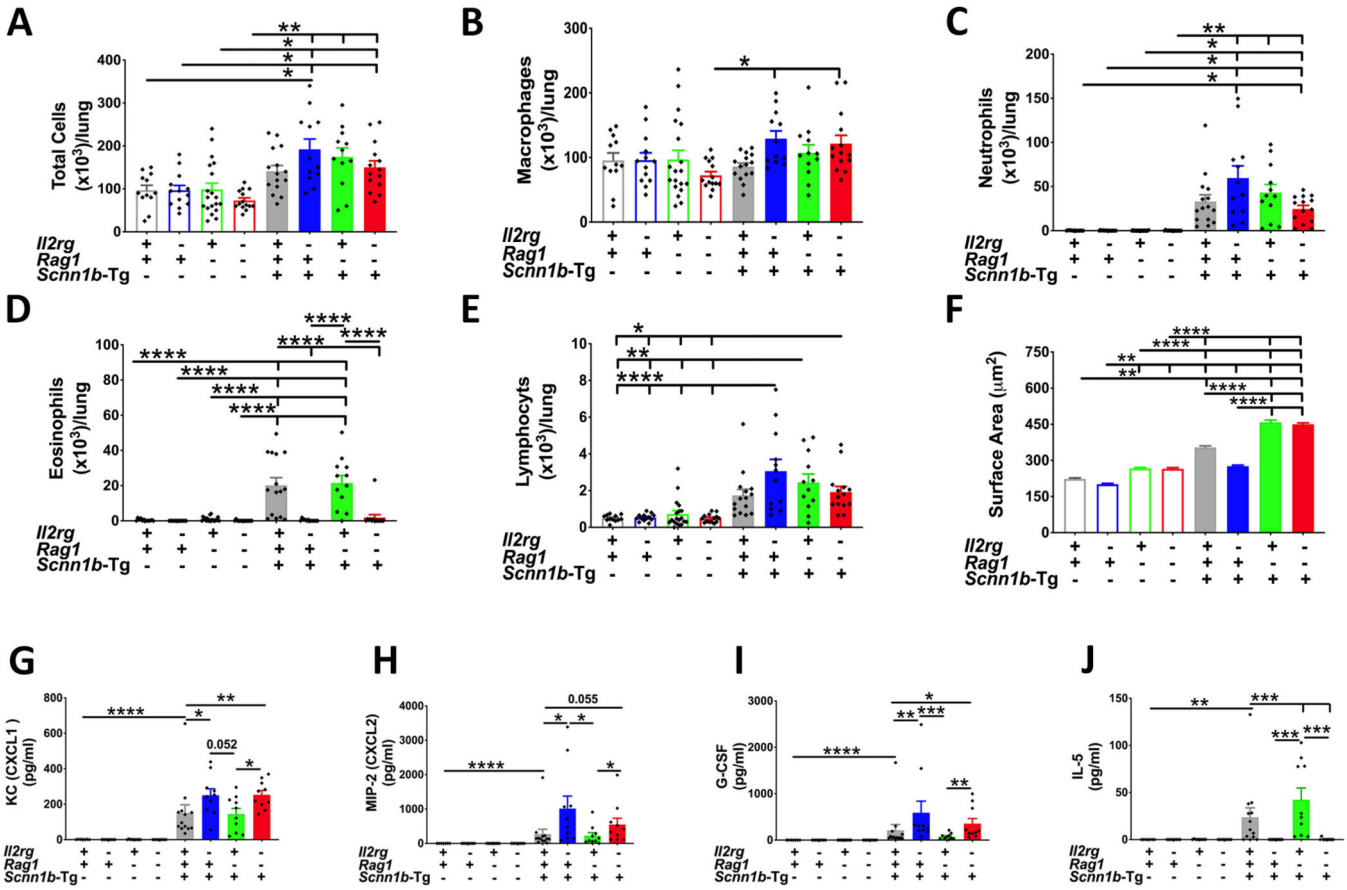

Figure 4: Ablation of ILCs does not affect immune cell recruitment.

Total cell counts **(A),** macrophages **(B)**, neutrophils **(C)**, eosinophils **(D)**, and lymphocytes **(E)** in BALF from immunocompetent WT (open gray bar, n=12), *Il2rg*^{KO}/WT (open blue bar, n=13*)*, *Rag1*^{KO}/WT (open green bar, n=19), *Il2rg*^{KO}*/Rag1*^{KO}/WT (open red bar, n=14), immunocompetent Tg+ (solid gray bar, n=15), *Il2rg*^{KO}/Tg+ (solid blue bar, n=12), *Rag1*^{KO}/Tg+ (solid green bar, n=12), and *Il2rg*^{KO}*/Rag1*^{KO}/Tg+ (solid red bar, n=14) juveniles. **(F)** Quantification of macrophage surface area from BALF macrophages from immunocompetent WT (open gray bar, n=6), *Il2rg*^{KO}/WT *(*open blue bar, n=12*)*, *Rag1*^{KO}/WT (open green bar, n=6), *Il2rg*^{KO}*/Rag1*^{KO}/WT (open red bar, n=6), immunocompetent Tg+ (solid gray bar, n=5), *Il2rg*^{KO}/Tg+ (solid blue bar, n=6), *Rag1*^{KO}/Tg + (solid green bar, n=6), and *Il2rg*^{KO}*/Rag1*^{KO}/Tg+ (solid red bar, n=6) juveniles. Cytokine levels (picogram per milliliter) of KC (CXCL1) **(G)**, MIP-2 (CXCL2) **(H)**, G-CSF **(I)** and, IL-5 **(J)** in cell-free BALF from immunocompetent WT (open gray bar, n=7), *Il2rg*^{KO}/WT *(*open blue bar, n=8*)*, *Rag1*^{KO}/WT (open green bar, n=9), *Il2rg*^{KO}*/Rag1*^{KO}/WT (open red bar, n=8), immunocompetent Tg+ (solid gray bar, n=13), *Il2rg*^{KO}/Tg+ (solid blue bar, n=10), *Rag1*^{KO}/Tg+ (solid green bar, n=10), and *Il2rg*^{KO}*/Rag1*^{KO}/Tg+ (solid red bar, n=10) juveniles. Error bars represent SEM. **p*<0.05; ***p*<0.01; ****p*<0.001; *****p*<0.0001 using ANOVA followed by Tukey's multiple comparison post-hoc test. KC, Keratinocyte chemoattractant; MIP-2, Macrophage inflammatory protein-2; G-CSF, Granulocyte-colony stimulating factor; IL-5, Interleukin-5.

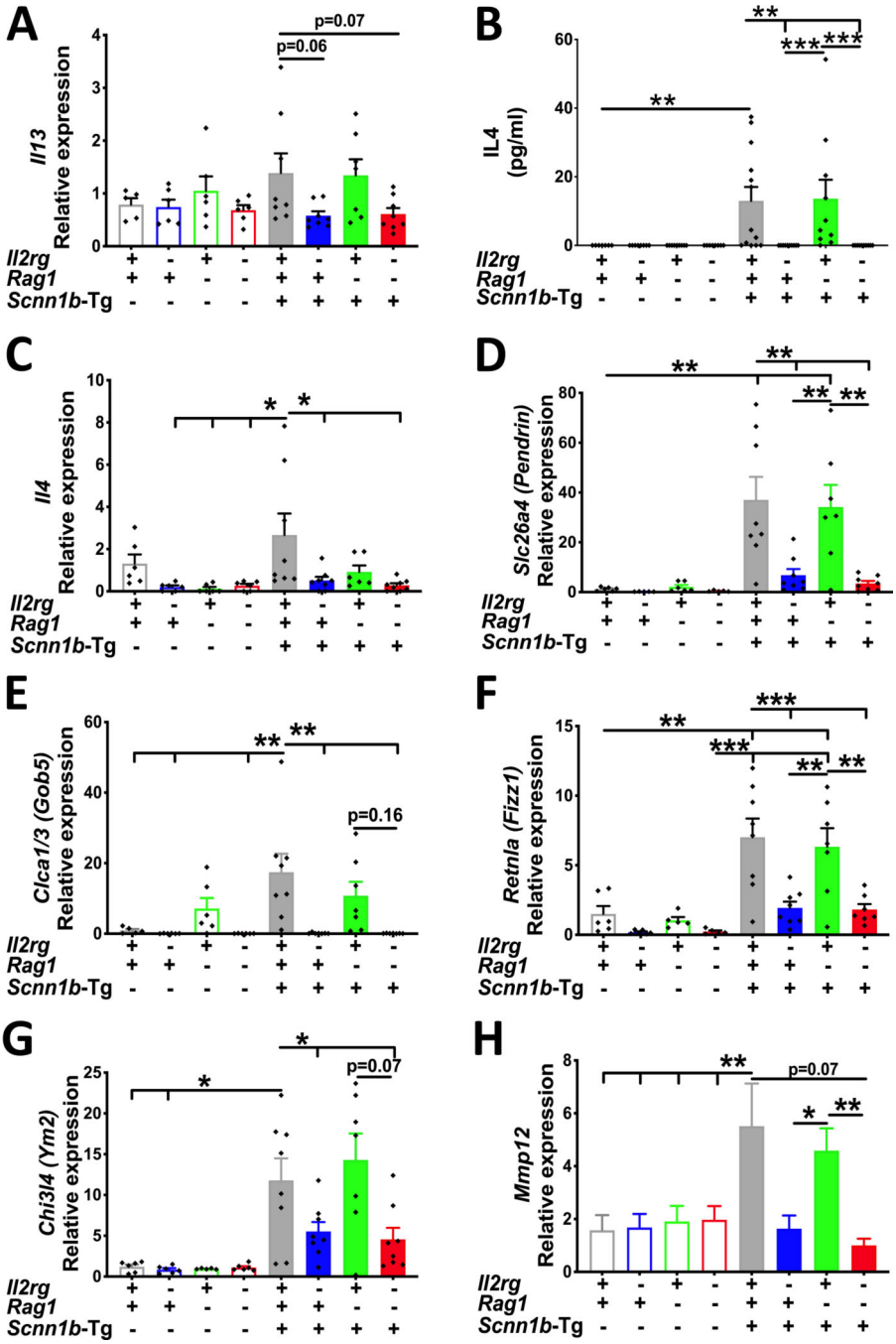

Figure 5: Ablation of innate lymphoid, but not of adaptive immunity, suppresses molecular signatures of Th2 inflammation in the airspaces of Tg+ juveniles.

(A) Relative quantification of *Il13* mRNA expression in total lung RNA isolated from immunocompetent WT (open gray bar), $Il2rg^{KO}$/WT (open blue bar), $Rag1^{KO}$/WT (open green bar), $Il2rg^{KO}/Rag1^{KO}$/WT (open red bar), immunocompetent Tg+ (solid gray bar), $Il2rg^{KO}$/Tg+ (solid blue bar), $Rag1^{KO}$/Tg+ (solid green bar), and $Il2rg^{KO}/Rag1^{KO}$/Tg+ (solid red bar) juveniles (n=5–8 mice per group). **(B)** Secreted levels (picogram per milliliter) of IL-4 in cell-free BALF from immunocompetent WT (open gray bar), $Il2rg^{KO}$/WT (open

blue bar), *Rag1*^{KO}/WT (open green bar), *Il2rg*^{KO}/*Rag1*^{KO}/WT (open red bar), immunocompetent Tg+ (solid gray bar), *Il2rg*^{KO}/Tg+ (solid blue bar), *Rag1*^{KO}/Tg+ (solid green bar), and *Il2rg*^{KO}/*Rag1*^{KO}/Tg+ (solid red bar) juveniles (n=7–13 mice per group). Relative quantification of *Il4* **(C)**, *Slc26a4* (*Pendrin*) **(D)**, *Clca1/3* **(E)**, *Retnla* (*Fizz1*) **(F)**, *Chi3l4* (*Ym2*) **(G)**, and *Mmp12* **(H)** mRNA expression in total lung RNA isolated from immunocompetent WT (open gray bar), *Il2rg*^{KO}/WT (open blue bar), *Rag1*^{KO}/WT (open green bar), *Il2rg*^{KO}/*Rag1*^{KO}/WT (open red bar), immunocompetent Tg+ (solid gray bar), *Il2rg*^{KO}/Tg+ (solid blue bar), *Rag1*^{KO}/Tg+ (solid green bar), and *Il2rg*^{KO}/*Rag1*^{KO}/Tg+ (solid red bar) juveniles (n=5–8 mice per group). Error bars represent SEM. *p<0.05; **p<0.01; ***p<0.001; using ANOVA followed by Tukey multiple comparison post-hoc test. *Il13,* Interleukin 13 mRNA; *Slc26a4*, Solute carrier family 26 member 4; *Clca1/3*, Calcium-activated chloride channel regulator 1; *Retnla*, Resistin-like molecule α; *Chi3l4*, Chitinase 3-like 4; *Mmp12*, Matrix metalloproteinase 12.

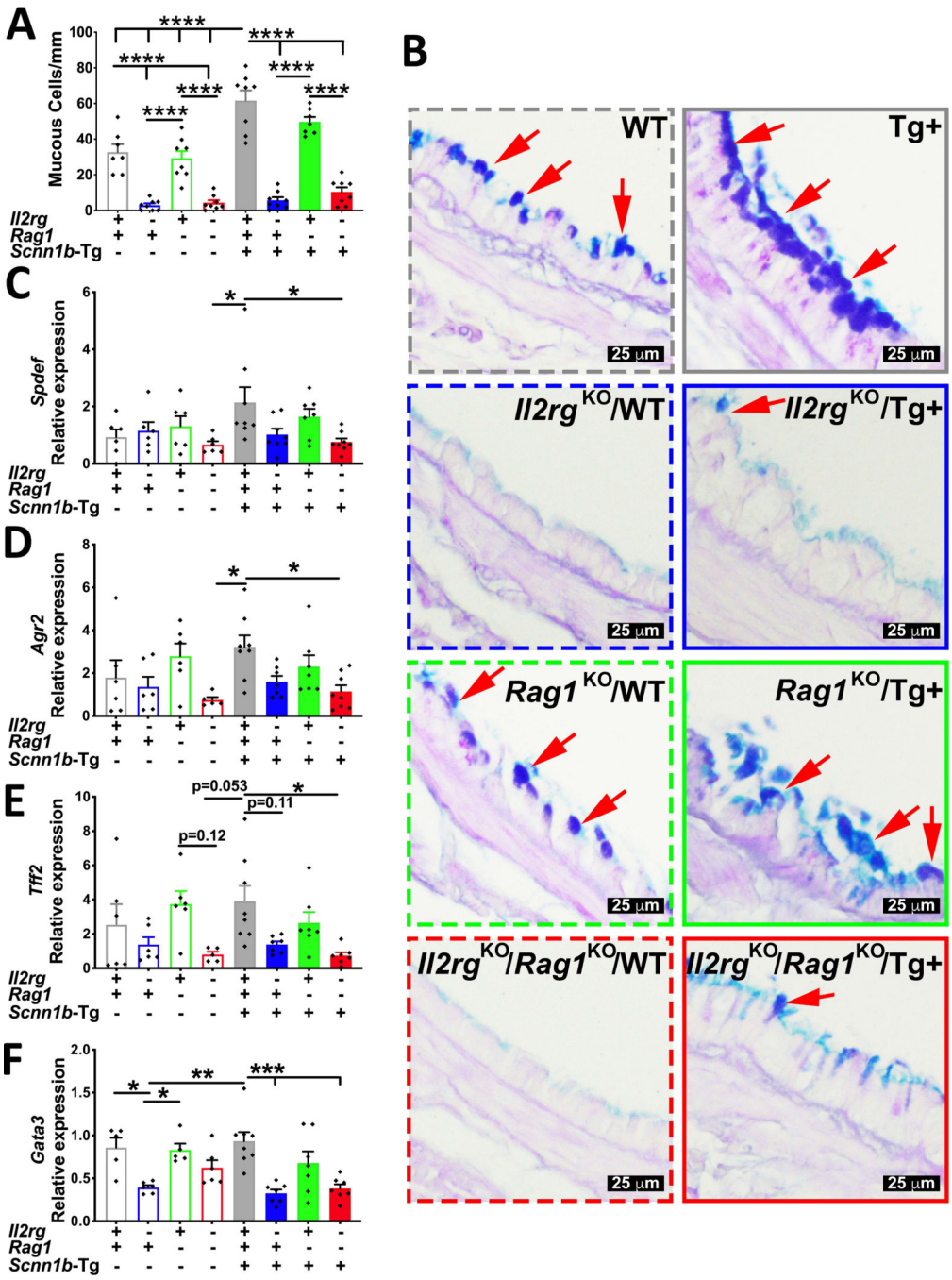

Figure 6: Ablation of innate lymphoid, but not of adaptive immunity suppresses mucous cell metaplasia in Tg+ juveniles.

(A) Quantification of mucous cells per millimeter of basement membrane from AB-PAS stained sections from immunocompetent WT (open gray bar), *Il2rg*^{KO}/WT (open blue bar), *Rag1*^{KO}/WT (open green bar), *Il2rg*^{KO}/*Rag1*^{KO}/WT (open red bar), immunocompetent Tg+ (solid gray bar), *Il2rg*^{KO}/Tg+ (solid blue bar), *Rag1*^{KO}/Tg+ (solid green bar), and *Il2rg*^{KO}/*Rag1*^{KO}/Tg+ (solid red bar) juveniles. (n=6–8 mice per group) **(B)** Representative photomicrographs from AB-PAS stained left lung lobe sections depicting AB-PAS positive

cells (red arrows). Relative quantification of *Spdef* **(C)**, *Agr2* **(D)**, *Tff2* **(E)**, and *Gata3* **(F)** mRNA expression in whole lung homogenates from immunocompetent WT (open gray bar), $Il2rg^{KO}$/WT (open blue bar), $Rag1^{KO}$/WT (open green bar), $Il2rg^{KO}/Rag1^{KO}$/WT (open red bar), immunocompetent Tg+ (solid gray bar), $Il2rg^{KO}$/Tg+ (solid blue bar), $Rag1^{KO}$/Tg+ (solid green bar), and $Il2rg^{KO}/Rag1^{KO}$/Tg+ (solid red bar) juveniles (n= 5–8 mice per group). *p <0.05; **p<0.01; ***p<0.001; ****p<0.0001 using ANOVA followed by Tukey multiple comparison post-hoc test. Error bars represent SEM. AB-PAS, Alcian blue-periodic acid Schiff; *Spdef*, SAM pointed domain containing ETS transcription factor; *Agr2*, Anterior gradient 2; *Tff2,* Trefoil factor 2; *Gata3,* GATA3 binding protein 3

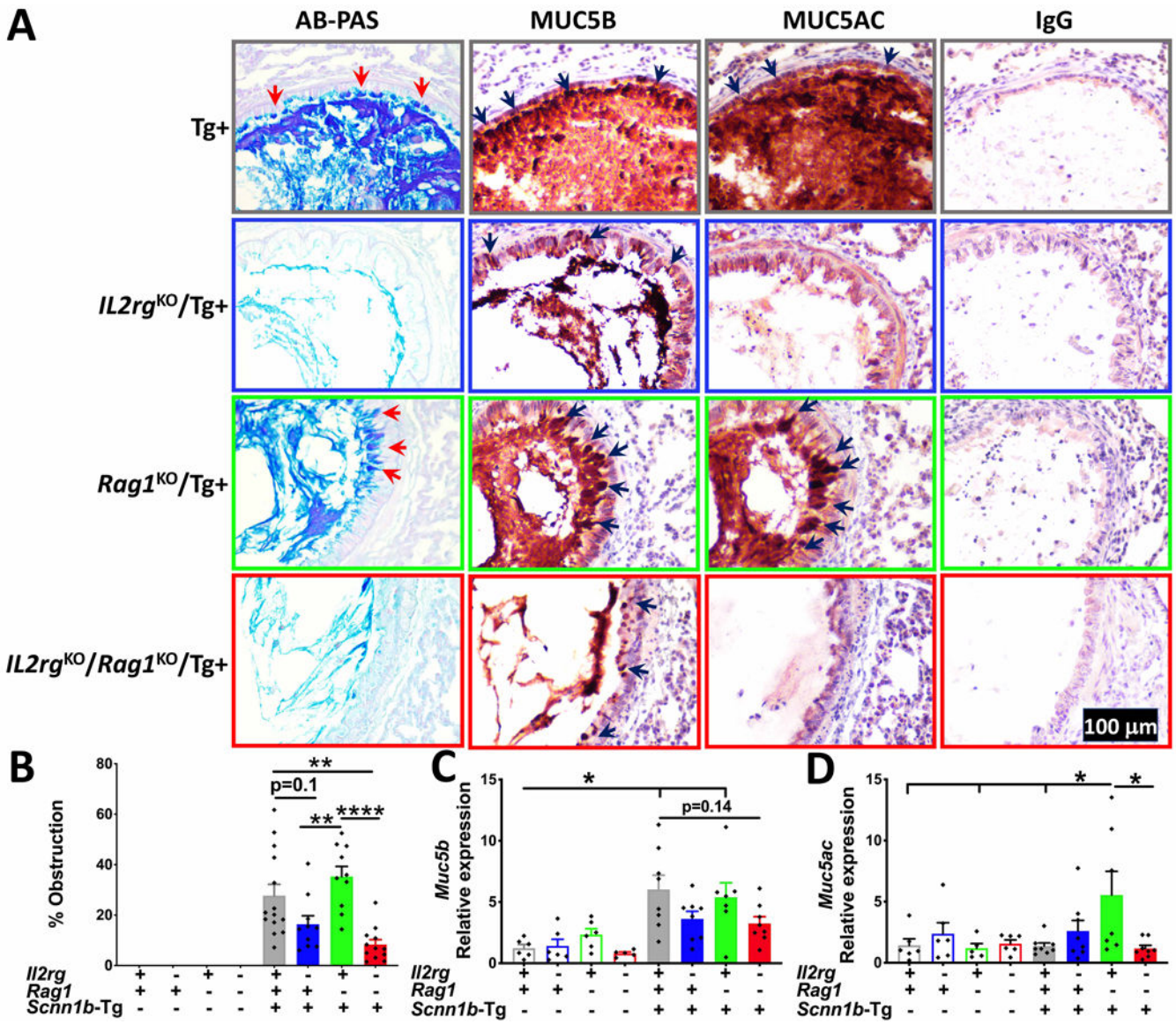

Figure 7: Ablation of innate lymphoid system mitigates mucus obstruction.

Representative photomicrographs of AB-PAS (**A**; first column), MUC5B (**A**; second column), MUC5AC (**A**; third column), and control IgG (**A**; fourth column) stained lung sections from immunocompetent Tg+, *Il2rg*^{KO}/Tg+, *Rag1*^{KO}/Tg+, and *Il2rg*^{KO}/*Rag1*^{KO}/Tg+ juveniles. **(B)** Quantification of airway mucus obstruction from AB-PAS-stained left lung lobe histological sections from immunocompetent WT (open gray bar), *Il2rg*^{KO}/WT (open blue bar), *Rag1*^{KO}/WT (open green bar), *Il2rg*^{KO}/*Rag1*^{KO}/WT (open red bar), immunocompetent Tg+ (solid gray bar), *Il2rg*^{KO}/Tg+ (solid blue bar), *Rag1*^{KO}/Tg+ (solid green bar), and *Il2rg*^{KO}/*Rag1*^{KO}/Tg+ (solid red bar) juveniles (n=8–11mice per group). Relative quantification of *Muc5b* **(C)** and *Muc5ac* **(D)** mRNA expression in whole lung homogenates from immunocompetent WT (open gray bar), *Il2rg*^{KO}/WT (open blue bar), *Rag1*^{KO}/WT (open green bar), *Il2rg*^{KO}/*Rag1*^{KO}/WT (open red bar), immunocompetent Tg+ (solid gray bar), *Il2rg*^{KO}/Tg+ (solid blue bar), *Rag1*^{KO}/Tg+ (solid green bar), and *Il2rg*^{KO}/

Rag1^{KO}/Tg+ (solid red bar) juveniles (n=5–8 mice per group). Error bars represent SEM. *p<0.05; **p <0.01 ****p <0.0001; using ANOVA followed by Tukey's multiple comparison post-hoc test.

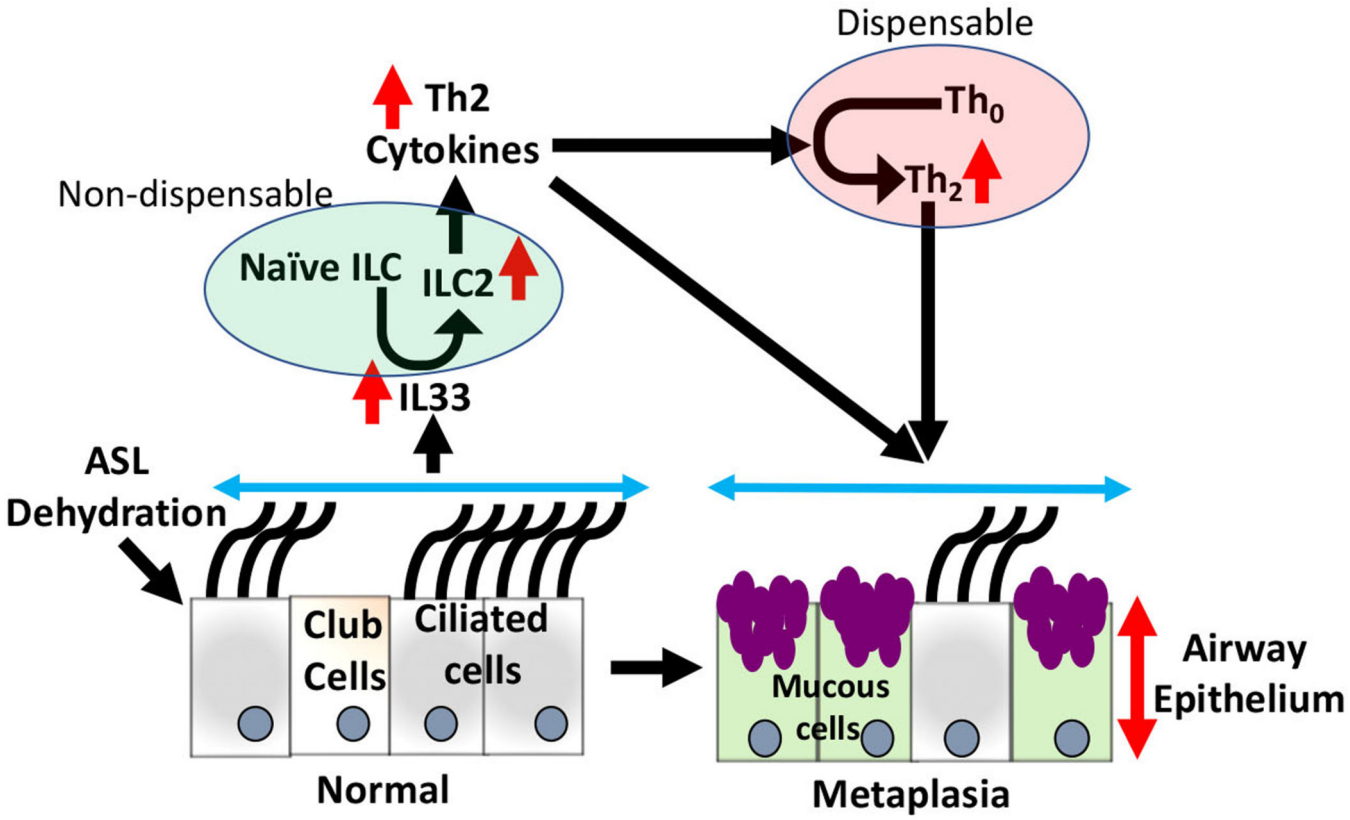

Figure 8: Interaction between innate lymphoid and adaptive immune system in the manifestation of ASL layer depletion associated mucous cell metaplasia.

ASL liquid dehydration exhibited in *Scnn1b*-Tg+ mice lead to IL-33 secretion. Through ST2, IL33 stimulates activation of ILC2s and production of Th2-associated cytokines, further facilitating differentiation of naïve *Th* cells into *Th2* cells. Th2-associated responses result in increased mucous cell metaplasia (MCM), mucus production, and airway obstruction. Adaptive immune cells are not essential in the MCM responses. Innate lymphoid immune cells are indispensable in the pathogenesis of muco-inflammatory airway disease. ILC2, Innate lymphoid cell 2, *Th2*, T-helper 2; MCM, Mucous cell metaplasia.